1   **The lithium isotope response to the variable weathering of soils in Iceland**

2

3   Philip A.E. Pogge von Strandmann[1,2*], Kevin W. Burton[3], Sophie Opfergelt[4], Bianca

4   Genson[2], Rannveig A. Guicharnaud[5], Sigurður R. Gislason[6]

5

6   [1]Institute of Geosciences, Johannes Gutenberg University, 55122 Mainz, Germany.

7   [2]Institute of Earth and Planetary Sciences, University College London and Birkbeck,

8   University of London, Gower Street, London, WC1E 6BT, UK.

9   [3]Department of Earth Sciences, Durham University, Durham, DH1 3LE, UK.

10   [4]Earth and Life Institute, Université catholique de Louvain, Croix du Sud 1 bte L7.05.10,

11   1348 Louvain-la-Neuve, Belgium.

12   [5]Icelandic Institute of Natural History, Urriðaholtsstræti 6-8, 210 Garðabær, Iceland.

13   [6]Institute of Earth Sciences, University of Iceland, Reykjavik, Iceland.

14

15   *Corresponding author: ppoggevo@uni-mainz.de

16

17

18   <u>Abstract</u>

19   This study has analysed Li isotopes ratios from well-studied soil and pore water

20   profiles from Iceland that have the same parent material but have experienced different

21   degrees of chemical weathering. Thus, from least to most weathered, we have analysed

22   vitrosols (V), gleyic andosols (GA), brown andosols (BA), Histosols (H) and Histic Andosols

23   (HA). Although the most weathered H and HA soils have the highest content in clay-sized

24   material, they have the least fractionated $\delta^7Li_{pore\ water}$ values. In contrast, the least weathered

25   GA and BA pore waters are most fractionated for Li isotopes. Given that Li isotope ratios are

26   fractionated by clay mineral formation, this appears counter-intuitive. A single trend for all

27   samples of δ^7Li as a function of Li/Na ratios suggests that they are all controlled by a process

28   with a single fractionation factor, in this case likely the formation of poorly-crystalline

29   allophane, which dominates in the "least weathered" soils. This rapidly forming secondary

30   mineral dominates Li isotope fractionation over more slowly-forming crystalline clays. The

31   fractionation along a single path shows that the key process here in controlling the Li isotope

32   ratio of surface waters is the degree of Li uptake by secondary minerals. This does not

33   necessarily correspond to the amount of clay minerals present in the soil, but to the amount of

34   clay minerals that are being newly formed in a single passage of the pore water through the

35   soil, or are in equilibrium with soil solutions at the time of sampling.

36

37   <u>1.0 Introduction</u>

38   The chemical weathering of rocks at the Earth's surface is the primary control on

39   atmospheric CO_2 levels on varying timescales. Weathering provides both alkalinity

40   (stemming from water-rock-atmospheric-carbon interactions) and cations for the formation of

41   marine carbonates, sequestering carbon (Berner et al., 1983; Walker et al., 1981). If the rocks

42   being weathered are silicates, containing virtually no carbon, then this carbon sequestration is

43   a net sink and a primary long-term climate controlling process. At the same time, continental

44   weathering provides a number of critical nutrients (e.g. iron, silicon, phosphorus) to the

45   coastal oceans, which stimulates primary productivity (Hawley et al., 2017; Lalonde et al.,

46   2012). This productivity temporarily also takes up atmospheric carbon, but most marine

47   organic matter is reoxidised before it is buried in marine sediments. However, continental

48   chemical weathering and physical erosion also provide clay particles into the coastal oceans.

49   These both increase nutrient fluxes to primary productivity (because microbes leach nutrients

50   from the rock particles (Grimm et al., 2019)), but, critically, also greatly increase organic

51 carbon burial, thus also sequestering carbon on the long term (Kennedy et al., 2014; Kennedy

52 and Wagner, 2011). Overall, this makes silicate weathering the primary atmospheric CO_2

53 controlling process on both long (via carbonate precipitation) and short, seasonal timescales

54 (via organic carbon burial).

55   Significant effort has focused on understanding and quantifying weathering processes

56 and fluxes, as well as on the processes that control weathering (Gislason et al., 2009; Maher,

57 2011; West et al., 2005). In particular, a feedback control, via a temperature-driven

58 "thermostat" is likely to be the overarching process that has mitigated climate over geological

59 time, although time periods also exist where an increase in supply may have overridden this

60 climate stabilisation process, such as in the Cenozoic (Raymo and Ruddiman, 1992).

61   The debates on these various processes have been at the forefront of biogeochemistry

62 for almost four decades, but finding reliable and unambiguous tracers of weathering

63 processes both in the present and geological past has proven tricky. One of the most

64 established of such tracers is lithium isotopes. Lithium is a moderately incompatible trace

65 element that is present in all silicate rocks, in orders of magnitude more than in carbonate

66 rocks (Penniston-Dorland et al., 2017; Pogge von Strandmann et al., 2020). Hence, in

67 weathering environments, Li arises from the dissolution of silicates, even in carbonate-

68 dominated catchments (Kisakürek et al., 2005; Millot et al., 2010). Lithium isotopes (^{6}Li and

69 ^{7}Li) are not fractionated by primary productivity (Pogge von Strandmann et al., 2016), and

70 while it remains poorly understood whether plants fractionate Li isotopes, the Li

71 concentration of plants is sufficiently low for surface waters to remain largely unaffected

72 (Clergue et al., 2015; Lemarchand et al., 2010; Li et al., 2020; Steinhoefel et al., 2021).

73 Instead, Li isotopes are fractionated by the silicate weathering process, in that when primary

74 silicate rocks (with a relatively low isotope ratio) are dissolved, they impart a low (rock-like)

75 δ^7Li to waters. Isotopically light lithium is preferentially taken up by formation of secondary

76 minerals (clays, oxides, zeolites), as well as by adsorption onto secondary minerals, imparting

77 a heavy isotopic signature to residual waters (Chan et al., 1992; Hindshaw et al., 2019; Huh et

78 al., 2001; Millot et al., 2010; Pistiner and Henderson, 2003; Pogge von Strandmann et al.,

79 2019a; Pogge von Strandmann et al., 2017b; Pogge von Strandmann and Henderson, 2015;

80 Teng et al., 2010; Vigier et al., 2008). Consequently, dissolved Li isotopes are controlled by

81 the weathering congruency: congruent dissolution of silicates imparts a low δ^7Li, while

82 incongruent weathering (where secondary minerals form) yields a high δ^7Li signature relative

83 to the parent material (Misra and Froelich, 2012; Pogge von Strandmann and Henderson,

84 2015).

85   Li isotopes are now well established as a tracer of both present and past weathering

86 processes (Dellinger et al., 2015; Hathorne and James, 2006; Lechler et al., 2015; Misra and

87 Froelich, 2012; Pogge von Strandmann et al., 2021a; Pogge von Strandmann et al., 2017a;

88 Pogge von Strandmann et al., 2013), but important questions remain, especially concerning

89 precisely how Li isotopes respond to changes in weathering processes. For example, the

90 effect of water-rock interaction time (e.g. secondary mineral formation rates) on Li isotopes

91 remains poorly quantified, partly because the timing of adsorption vs. incorporation during

92 neoformation is poorly known, and because the effect of Li uptake by oxides/oxyhydroxides

93 vs. clay or zeolites is also poorly known (Hindshaw et al., 2019; Li and Liu, 2020). This

94 study aims to investigate the, as yet, little quantified effects arising from variable degrees of

95 weathering in soils – for example, high solution δ^7Li could be due to either a high fraction of

96 removal with a low fractionation factor, or lower removal with a high fractionation factor.

97 Here we examine soil and pore water profiles from different soil types from Iceland. These

98 different profiles represent weathering of bedrock with a similar composition, but reflect

99 differing degrees of weathering.

100

101 <u>2.0 Samples</u>

102   Five different Icelandic soil types were analysed that represent increasing degrees of

103 chemical weathering, collected in 2009 and 2010 (Opfergelt et al., 2014), and are shown on a

104 soil map of Iceland (Fig. 1). These particular samples have previously been analysed for the

105 isotopes of Mg, Si, Fe and Zn (Opfergelt et al., 2014; Opfergelt et al., 2017a; Opfergelt et al.,

106 2017b). These Icelandic soils have specific definitions (Arnalds, 2004): Vitrisols (V)

107 represent the least weathered soils from Iceland, and have <1% organic carbon or <1% Si_{ox}.

108 Their mineralogy is dominated by volcanic glass, and they have little (5–10%) plant cover.

109 Broadly, they represent a desert-like environment with little vegetation or soil formation, but

110 in a cold and wet environment.

111   Gleyic andosols (GA – where US spelling is Andisols) are slightly more weathered,

112 and tend to have organic carbon contents (<12%) in surface horizons. They contain allophane

113 contents of up to 20%.

114   Brown andosols (BA) are increasingly weathered, and are the classical freely drained

115 andosols found in Iceland. They tend to contain significant allophane (15–30%), as well as

116 some ferrihydrite (1–8%).

117   Histosols (H) and Histic Andosols (HA) are the most weathered soils in this study.

118 Histosols are dominated by organic materials (>20% organic C). Histic Andosols are found in

119 poorly drained areas, and have sufficient aeolian inputs to reduce their organic contents

120 below the 20% limit for Histosols. Allophane content is 2–10%, and they meet the (Al +

121 $0.5Fe)_{ox}$ criteria for Andosols.

122   Overall, Iceland is covered by ~48% Andosols (of all types), ~40% Vitrisols and

123 Leptosols and ~1% Histosols (and 11% by glaciers and ice caps) (Arnalds, 2004). In general,

124 vegetated areas are dominated by Andosols, desert areas by Vitrisols and wetlands by

125 Histosols.

126   In this study, the vitrisol (V) is from SW Iceland, located south of the Langjökull and

127 west of the Myrdalsjökull ice caps. The gleyic andosol (GA) is from just north of Reykjavik.

128 The brown andosol (BA), the Histosol (H), and the Histic Andosol (HA) are from the

129 Borgarfjörður catchment in western Iceland. Peats were developed at the HA and H sites

130 (Opfergelt et al., 2014). Overall, GA and BA soils are well-drained, while the H and HA soils

131 are poorly drained, with inevitable consequences for the water-rock interaction time. All soils

132 developed from similar tholeiitic basalt, and their difference from each other is largely due to

133 the soil drainage conditions (Opfergelt et al., 2014).

134   Further to the soils, a series of local secondary minerals was acquired from the

135 Natural History Museum in Reykjavik. These minerals were not always formed in the same

136 areas as the soils (although many are from the same catchment), but are from similar

137 Icelandic weathering environments, and are examined here to provide some context of

138 secondary mineralogy. These include samples of different calcites, clays (unidentified) and

139 six different types of zeolite (heulandite, chabazite, mesolite, stilbite, epistilbite and

140 scolecite). Further, an Fe-oxyhydroxide was taken from the coating on a pebble from a side

141 stream on the nearby Norðura River (locality A6; (Pogge von Strandmann et al., 2006)). The

142 major element composition suggests that this coating is largely impure ferrihydrite,

143 containing Al, P and possibly Si admixtures (Si not measured), typical of soil and stream

144 environments, but the presence of other phases, such as Al-hydroxide, cannot be ruled out.

145

146 <u>3.0 Methods</u>

147 *3.1 Sampling*

148   Sampling is described in Opfergelt et al. (2014). Briefly, typical parent tholeiitic

149 basalt was sampled at the BA site. This represents the type of parent material for the HA, H,

150 BA and GA sites. For the Vitrisol, the C horizon was considered as unweathered parent

151 volcanic ash. Soil profiles were described following FAO guidelines and sampled by horizon.

152 Soil samples were air-dried and sieved at 2mm. The measurement of chemical and physical

153 properties of the soils (pH, cation exchange capacity (CEC), chemical composition) is

154 described by Opfergelt et al. (2014).

155   Three representative soils were sequentially leached to separate out different phases,

156 and analysed for Li concentrations. The leaching technique followed a modified version of

157 Tessier et al. (1979) detailed in Revels et al. (2021). Briefly, the exchangeable fraction was

158 leached using $Mg(NO_3)_2$ at pH5 for 1 hour; carbonates were leached using acetic acid

159 buffered with Na acetate to pH5 for 5 hours; oxides were leached using NH_2OH-HCl in

160 acetic acid at 96°C; the silicate residue was dissolved using the method described for bulk

161 soils below.

162   Soil solutions were sampled over two different seasons (September 2009 and June

163 2010), using macro rhizon soil water samplers, which filter pore waters at 0.2 μm. Elemental

164 concentrations were determined by ICP-MS and ion chromatography, as described by

165 Opfergelt et al. (2014). In their initial measurements, Li concentrations were not always

166 determined, because [Li] was so low, and was hence below detection limits. For these

167 samples, Li concentration was re-determined by this study during isotope analysis, by drying

168 down at least 10ml of sample, and comparing the MC-ICP-MS beam intensity to that of a

169 known concentration standard.

170

171 *3.2 Li isotope analyses*

172   Lithium isotope purification and analyses by our methods have been described in

173 elsewhere (Pogge von Strandmann et al., 2011; Pogge von Strandmann and Henderson,

174 2015). Briefly, soils were dissolved in HF-HNO_3-$HClO_4$, HNO_3 and HCl, and sufficient pore

175 water was dried down to attain 20ng Li. This was purified through a two-step cation

176   exchange method, and analysed relative to the LSVEC standard on a Nu Instruments HR

177   MC-ICP-MS at Oxford University. Splits taken before and after the Li collection bracket on

178   the columns show that >99.9% of Li analysed, which is essential for both precision and

179   accuracy. The total procedural blank for Li isotopes is effectively undetectable (<0.005 ng

180   Li). Long-term precision of this method and instrument is ±0.6‰ (2sd), based on repeated

181   seawater analyses of 31.2 ± 0.6‰ (2sd, n = 62), and BCR-2 basalt of 2.6 ± 0.4‰ (n = 6).

182

183   4.0 Results

184   Opfergelt et al. (2014) extensively characterised these soils, and results are given in

185   Tables 1 and 2. Briefly, the primary mineralogy of these soils (augite, Ca-plagioclase,

186   magnetite) reflects that of the primary tholeiitic basalt. Based on selective extraction,

187   secondary minerals are dominated by short-range ordered minerals, mainly allophane and

188   ferrihydrite, as also reported from other Icelandic soils (Arnalds, 2004; Sigfússon et al., 2006,

189   2008). No other secondary minerals were identified in the soils' clay-sized fraction (<2μm),

190   except in the HA soil, where XRD detected smectite and kaolinite (Opfergelt et al., 2014).

191   The allophane content is higher in the V-BA-GA soils than in the HA-H soils. This is because

192   allophane forms above pH 4.9 when Al is not complexing with humus and therefore the more

193   acidic HA-H soils have a lower allophane content (Mizota and van Reeuwiik, 1989). The

194   HA-H soils do contain some allophane, which is explained by aeolian deposition or by higher

195   pH conditions that may have existed earlier in the soil development cycle (Opfergelt et al.,

196   2014).

197   As described by Opfergelt et al. (2014), one of the primary chemical properties of the

198   bulk soils is the total reserve in bases (TRB = [Na] + [Mg] + [Ca] + [K]). The TRB is well-

199   defined as a relative index quantifying the leaching of these cations in the soils relative to the

200   parent material (e.g. Ameijeiras-Mariño et al., 2017; Delvaux et al., 1989; Henriet et al.,

201   2008), and hence provides an estimate of the content of the weatherable minerals in the soils.

202   Any fraction of cations that are included in present secondary, rather than primary minerals,

203   will still be included in the TRB. The TRB value in soils decreases with increased

204   weathering, and leads to the observation that the least weathered soil is the Vitrisol (average

205   TRB = 618 cmol$_c$/kg), compared to a value of 733 cmol$_c$/kg in the pristine basalt, followed by

206   the Gleyic Andosol (TRB = 401 cmol$_c$/kg), then the Brown Andosol (TRB = 358 cmol$_c$/kg),

207   then the Histosol (TRB = 194 cmol$_c$/kg), closely followed by the Histic Andosol (TRB = 158

208   cmol$_c$/kg), which is therefore the most weathered soil type. This relative degree of weathering

209   is supported by a direct correlation with the proportion of free Fe (Fe$_d$/Fe$_t$) (Opfergelt et al.,

210   2017b), which is also used as a weathering indicator. This is also further supported by the

211   total clay-sized content (<2μm), which is higher in the HA-H soils (53 and 43%,

212   respectively) compared to the BA-GA (both ~35%) and V (4.6%) soils (Table 1).

213

214   *4.1 Lithium in soils*

215   None of the soil profiles have a clear trend in Li concentrations with depth (Fig. 2a).

216   Overall, the GA soil has the highest Li concentrations (10.6 ± 2.8 (1sd) μg/g), followed by

217   the BA and V (8.3 ± 2.6 and 8.3 ± 3.0 μg/g, respectively), and then by the H and HA (5.2 ±

218   3.3 and 5.2 ± 2.8 μg/g, respectively). In comparison, the host basalt has a Li concentration of

219   5.89 μg/g, within the range for Icelandic basalts (Pogge von Strandmann et al., 2006; Pogge

220   von Strandmann et al., 2008; Pogge von Strandmann et al., 2012; Vigier et al., 2009).

221   The selective leaches of three soils (HA O1, H O6, BA BW2) show that between 0.2

222   and 3.4% of the total Li is in the exchangeable fraction, slightly less than observed during

223   experiments with Icelandic basalts (Pogge von Strandmann et al., 2019a), but similar to the

224   amount of Mg reported in this fraction (Opfergelt et al., 2014). Carbonates contain a similar

225   proportion of Li (1–4%). The oxide fractions (primarily Fe-oxides) contain significantly more

226 Li, ranging from 10% in the BA soil, to 25% in the HA soil. The silicate fraction contains

227 ~90% of the total Li in the BA soil, 70% in the HA soil, and 72% in the H soil (Table 1).

228 Although the recovered phases are slightly different compared to the BCR leaching of

229 Hawaiian basalt by Li et al. (2020) (e.g. that method combines exchangeable and carbonate

230 phases in a single leach), the results agree in that the silicate fraction dominates the Li budget,

231 followed by the oxide fraction. The least weathered leached soil (BA) has the least Li in any

232 of the secondary fractions.

233   Similarly, there are no trends with depth for soil δ^7Li, except for the BA, where δ^7Li

234 decreases linearly from 6.4 to 2.1‰ with increasing depth (Fig. 3). There is, however, a

235 difference in the average δ^7Li_{soil} between different soil types. From least to most weathered,

236 the V soil has an average of 1.9 ± 1.9‰, the GA of 5.2 ± 1.3‰, the BA of 2.7 ± 3.0‰, and H

237 of -0.2 ± 3.5‰ and the HA of 0.5 ± 1.4‰. In other words, aside from the Vitrisol, the

238 average δ^7Li_{soil} decreases as the degree of weathering increases. The parent basalt has a δ^7Li

239 of 3.6‰, within the range for Icelandic basalts and MORB. In particular, this parent value is

240 similar to that of 2010 Eyjafjallajökull ash (3.9‰; Pogge von Strandmann et al., 2012)), of

241 unaltered basalt at the Reykjanes Peninsular (3.7‰; Verney-Carron et al., 2015)), and

242 elsewhere in Iceland (3.1–4.0‰; Ryan and Kyle, 2004)), suggesting that there is little

243 variability across Iceland, and hence of the parent composition of our different soil profiles.

244

245 *4.2 Lithium in pore waters*

246   No pore waters exist from the very fast-draining Vitrisol. In the other soils, there is a

247 hint of increasing Li concentrations with depth in the HA and BA (Fig. 2b), but not in the

248 other soil profiles. On average, the Li concentrations increase with increasing degree of

249 weathering: the GA has an average pore water Li concentration of 0.09 ± 0.02 ng/ml,

250 compared to 0.15 ± 0.07 ng/ml in the BA, 1.78 ± 1.12 ng/ml in the HA and 3.27 ± 2.54 ng/ml

251   in the H. In comparison, Icelandic rivers range between 0.015 and 0.4 ng/ml, although up to

252   1.1 ng/ml in rivers with hydrothermal input (Pogge von Strandmann et al., 2006). A Histic

253   Andosol from elsewhere in Iceland has reported pore water Li concentrations of 0.67–1.94

254   ng/ml (Pogge von Strandmann et al., 2012).

255   There are sometimes significant differences between both the [Li] and the δ^7Li_{PW} (on

256   average ~10‰) from the same horizons, but from the two different years/seasons, collected

257   in September (late summer) 2009 and June (spring) 2010 (Fig. 3). Some variability between

258   shallow (<70cm) pore waters could be expected, given fluctuations in water-levels,

259   evaporation and redox variations, which could also explain the lack of consistent differences

260   between the different soils. Broad patterns appear to be maintained, however; for example, in

261   the HA, pore waters from both years trend towards lighter isotope ratios with depth (Fig. 3),

262   similarly to broadly flat profiles in the Gleyic Andosol.

263   Lithium isotope ratios show trends to lower values with depth in the HA and H

264   profiles, but not in the others. Overall, the pore water δ^7Li_{PW} is always higher than that of the

265   soils, except at the base of the HA soil, where pore waters become similar or even slightly

266   isotopically lighter than their corresponding soils. A precipitation correction (denoted by *) is

267   applied to the major element pore water data, based on the assumption that rainwater in

268   Iceland stems from the oceans (Pogge von Strandmann et al., 2006), and that all Cl^- in the

269   pore waters stems from marine aerosols, which is validated by the low Cl^- concentrations of

270   Icelandic basalt (Gíslason et al., 1996). We do not apply a precipitation correction to pore

271   water Li. This is because an attempted correction using seawater elemental ratios and isotope

272   compositions, and the measured [Cl], drives around a third of [Li] to negative values. We also

273   note that the pore water data do not lie on a mixing trend with seawater. This is a similar

274   approach to other basaltic Li studies (Liu et al., 2015; Pogge von Strandmann et al., 2006),

275   and we note that this may be due to analytical uncertainty in both [Cl] and [Li] values, as also

276   suggested by other studies (Pogge von Strandmann et al., 2010). We note that for samples

277   where the correction can be made, the contribution from sea spray is generally <10%, and

278   averages <5%.

279   Between different soil profiles there are large average δ^7Li_{PW} differences that

280   correlate with the degree of weathering. The least weathered GA has the highest δ^7Li_{PW} of

281   26.7 ± 3.4‰ (1sd). The BA has an average δ^7Li_{PW} of 23.2 ± 7.3‰, the H of 14.3 ± 3.3‰ and

282   the HA of 6.6 ± 6.9‰. In comparison, Icelandic (non-hydrothermal) rivers have a δ^7Li of

283   15.4–44‰ (Pogge von Strandmann et al., 2006; Pogge von Strandmann et al., 2016; Vigier et

284   al., 2009), and another reported Icelandic Histic Andosol has pore waters that have a δ^7Li

285   ranging between 7.4–21.4‰ (Pogge von Strandmann et al., 2012).

286

287   *4.3 Lithium in secondary minerals*

288   While the fluids that correspond to the secondary minerals are not available (although

289   most were formed in the same catchment as most of the soils analysed here), analysis of the

290   solid secondary minerals, nevertheless, provides some insight into their effect on lithium

291   behaviour (Table 1). Li concentrations in the calcites are similar at 32–39 ng/g, over two

292   orders of magnitude below Icelandic basalt. Of the silicate secondary minerals, the clays have

293   Li concentrations of ~5–14 μg/g, similar to that of the Fe oxyhydroxide (14 μg/g), but

294   significantly higher than the zeolites (0.4–2.7 μg/g).

295   Li isotope ratios in the calcites range between -1.0 and 5.4‰. Inorganic calcites are

296   reported to have fractionation factors of 3–6‰ from fluid (Marriott et al., 2004). The clays

297   exhibit a similarly wide variation in δ^7Li, with values of -8.4 and 2.1‰. The zeolites tend to

298   have fairly low δ^7Li values (-4.9 to -0.2‰), except for heulandite (7.9‰) and scolecite

299   (5.3‰). Given the differing locations and the variability in the pore waters detailed above, it

300   is not possible to determine fractionation factors from these samples. As such, the Li

301 concentrations potentially provide more information than the isotope ratios, supporting the

302 hypothesis that carbonate weathering does not significantly affect dissolved Li compared to

303 silicates (Kisakürek et al., 2005). In addition, the concentration data suggest that zeolites play

304 a more minor role in affecting Li behaviour than clays and Fe oxyhydroxides.

305

306 5.0 Discussion

307 *5.1 Elemental depletion in soils*

308   In Icelandic basalt weathering, Na is the most mobile major cation (Gíslason et al.,

309 1996), consequently it goes into solution preferentially over Mg and Ca, which are

310 approximately 10 times less mobile (Gíslason et al., 1996; Pogge von Strandmann et al.,

311 2006). Elemental depletion in soils can be assessed from τ calculations (Brimhall and

312 Dietrich, 1987; Chadwick et al., 1990), where the loss or gain of Li compared to the parent

313 material is compared to that of an immobile element. Positive τ values indicate a net

314 elemental gain, while negative ones indicate a loss. Here we use Zr as the immobile element,

315 although we note that τ values normalised to Nb yield values within ±10%. Mobile major

316 cations such as Mg and Ca have consistently negative τ values (aside from one sample for

317 Mg), showing that they have been stripped from the soils. The average τ values for Mg and

318 Ca from each soil sequence decrease with increasing weathering grade (Fig. 4a,b), agreeing

319 with the other tracers of the degree of weathering, such as TRB. The overall τ values for

320 these elements are higher than, for example, in the highly weathered bauxite profiles

321 developed in the Columbia River Basalts (Liu et al., 2013), which is to be expected in the

322 more kinetically-limited weathering regimes of Iceland (Dellinger et al., 2015).

323   More immobile elements, such as Al, also tend to have negative τ values in most of

324 the samples (apart from at the base of the GA soil), albeit significantly higher numbers than

325 the mobile elements. The Gleyic Andosol has values close to zero, and these values then

326 decrease with increasing grade of weathering in the other profiles (Fig. 4c). In other words,

327 some Al has been stripped from the more weathered of these soils, but considerably less than

328 the mobile elements, and overall elemental loss is less than in more weathered Columbia

329 River Basalt soil profiles (where τ_{Mg} values are uniformly close to -1, and τ_{Al} values average

330 at ~-0.55 (Liu et al., 2013)).

331

332 *5.2 Soil lithium isotopes*

333   Tau values were also calculated for Li, relative to Zr (Fig. 4d). Only the H and HA

334 soils show any Li loss, and it is the HA that shows the greatest Li loss (average $\tau_{Li,Zr}$ = -0.07 ±

335 0.6), while on average the Histosol has gained Li ($\tau_{Li,Zr}$ = 0.19 ± 0.7). The BA and GA soils

336 have gained even more Li (($\tau_{Li,Zr}$ = 0.27 ± 0.15 and 0.35 ± 0.28, respectively). The vitrisol

337 has a tau value close to 0 (0.06), reflecting its relatively unaltered status. Positive τ values are

338 in contrast to soil profiles from Hawaii and the Columbia River Basalts, where soils are

339 almost always depleted in Li, and tend to exhibit much lower absolute τ_{Li} values in both

340 settings (Liu et al., 2013; Ryu et al., 2014). Relative Li enrichment at depth in Hawaii,

341 especially in older soils, is reported as due to Li retained in secondary minerals (Ryu et al.,

342 2014). In the Icelandic soils examined here, the average τ_{Li} for each profile decreases with

343 increasing weathering grade (based on TRB, and other tracers mentioned above), meaning

344 that the nominally least weathered profiles are enriched in Li relative to the parental rock,

345 while more weathered profiles are comparatively depleted in Li. The Gleyic Andosol in

346 particular is increasingly enriched towards the base of the soil, and this mimics enrichment in

347 Al (Fig. 4c), confirming that Li is being retained by secondary minerals – in this case largely

348 allophane.

349   There is no direct relationship between the $\delta^7 Li_{soil}$ values of individual samples and

350 their τ_{Li} values. For example, both the Histic Andosol and especially the Histosol, show

351 layers that are relatively isotopically heavy compared to the rest of the soils (Fig. 3). In both

352 cases these correspond to ash layers. In the HA profile, the ash layer is mixed with a redox

353 layer of organic-rich material, while in the H profile it is pure ash.

354 Discounting those layers, however, there is a clear decrease in average δ^7Li_{soil} with

355 increasing level of weathering, except for the Vitrisol ($\delta^7Li = 1.9 \pm 1.9‰$), which overlaps

356 the composition of the parent basalt (3.6‰). Thus, δ^7Li values decrease from GA > BA > H ~

357 HA, which also broadly co-varies with the TRB values, although there is scatter within each

358 soil type. This also yields a positive co-variation between the average τ_{Li} and the $\Delta^7Li_{soil-basalt}$

359 (i.e. the difference in δ^7Li between the soil and the parent basalt) for each soil type (Fig. 5).

360 This trend is enhanced by highly depleted and isotopically light bauxites from the Columbia

361 River Basalts (Liu et al., 2013). Various Hawaiian soils also lie on this trend (Li et al., 2020;

362 Ryu et al., 2014), albeit with the humid profile from Li et al. (2020) having a large variability

363 (Fig. 5).

364 Isotopically lighter Li isotope ratios in soils could be taken to suggest a greater Li

365 accumulation in secondary minerals, relative to soils with heavier values (Clergue et al.,

366 2015; Pogge von Strandmann et al., 2012). However, in the case of these soils, those that are

367 enriched in Li relative to the parent basalt (positive τ_{Li}) are isotopically heavier compared to

368 those that are depleted in Li. There is also an overall positive co-variation between soil δ^7Li

369 and the abundance of clays such as allophane (Fig. 6a), which is the dominant secondary Al-

370 silicate in these environments (Opfergelt et al., 2014; Stefansson and Gislason, 2001; Wada et

371 al., 1992). There is no co-variation between δ^7Li_{soil} and the abundance of ferrihydrite nor

372 clay-sized contents (Fig. 6b), showing that in these environments, Li sorption on iron

373 oxyhydrides or incorporation into crystalline clays is not controlling isotope fractionation.

374 There is also is no correlation between soil δ^7Li and $\delta^{66}Zn$, where Zn is thought to be

375 controlled by the soil organic matter content (Opfergelt et al., 2017a), suggesting that Li

376 isotopes are not affected by organic matter, as also confirmed by other studies (Li et al.,

377 2020).

378   It therefore appears that the amount of total clay-sized material in the soils is not the

379 primary control on bulk soil δ^7Li values. The correlation between δ^7Li_{soil} and allophane

380 contents (and also δ^7Li_{soil} and τ_{Li}) is also hard to understand, because soil δ^7Li values extend

381 to values both higher and lower than those of unaltered basalt, or indeed Icelandic volcanic

382 ash (Pogge von Strandmann et al., 2012). Thus, it is unlikely that the isotopically light bulk

383 soils values of the H and HA are due to a low allophane content. Instead, as discussed below

384 (Section 5.3), it appears more likely that greater allophane content is associated with higher

385 δ^7Li values because the secondary minerals are precipitating from isotopically heavy soil

386 pore waters. In other words, greater clay formation is driving pore water δ^7Li higher, from

387 which secondary minerals are then precipitating. This can occur in a standard coupled

388 relationship of two reservoirs with a constant fractionation factor (Faure, 1986). It would,

389 however, also mean that the initial dissolution of basalt would at first yield secondary

390 minerals that are isotopically lighter than basalt. This initial isotopically lightest phase is not

391 being resolved here, however. Complete loss of this phase via erosion is relatively unlikely, if

392 this phase is an aluminosilicate, because allophane is the first of these phases to form

393 (Arnalds, 2004). Therefore, such a light phase would have to be of another composition, or,

394 more likely, is not resolvable in the analysis of bulk soils due to mass balance considerations.

395 This is discussed further below in the context of the pore waters.

396   An alternate hypothesis is that the least weathered soils (BA and GA) have a higher

397 δ^7Li because they have experienced a lower solid to solution partitioning of Li, i.e. a lower

398 weathering intensity. This can be tested by comparing the measured τ_{Li} value to those based

399 on a steady-state mass balance between the dissolved load, soil and bedrock. If modelled

400 (steady-state) τ_{Li} values are similar to measured values, it would imply that the system is in

401 steady-state, and weathering intensity (the Li in the water/solid ratio) is controlling the soil Li

402 gain or loss. In contrast, if modelled and measured values are not similar, then there is a

403 decoupling between the present-day solution and solids, and more rapidly forming secondary

404 minerals (i.e. allophane) are controlling solution compositions. We model τ_{Li} using equations

405 from Bouchez et al., 2013:

406 $$w = \frac{\delta_{soil} - \delta_{rock}}{\delta_{soil} - \delta_{diss}} = -\tau^{steady-state}$$

407 Where δ is the δ^7Li values of the soil, rock and dissolved load. Overall, there is no

408 relationship between the measured and modelled steady-state τ_{Li} values ($r^2 = 0.15$). However,

409 there is a positive co-variation for the HA soils (Fig. 7), while there is none for the other soil

410 types. This strongly suggests that the isotopically heavy soils (BA and GA) are not at steady-

411 state between their solutions and soils, whereas the HA soil may be. In turn, this suggests that

412 our previous hypothesis is correct, and the BA and GA soils exhibit decoupling between their

413 solutions and soils, and therefore their high δ^7Li may be due to allophane taking up Li from

414 heavy pore waters.

415

416 *5.3 Allophane control on pore water profiles*

417   These soils also exhibit a positive co-variation between δ^7Li_{PW} and allophane contents

418 (significant $p<0.01$ for Spearman Rank correlation; Fig. 8). Thus, while the total clay-sized

419 content co-varies negatively with δ^7Li_{PW} (greater clay-sized content in the poorly-drained

420 soils), the allophane content co-varies positively with δ^7Li_{PW} (greater allophane in the

421 rapidly-drained soils). This correlation is highly unlikely to be caused by redissolution of

422 isotopically light clay minerals, as observed in supply-limited regimes such as the tropics

423 (Dellinger et al., 2015), because weathering regimes in Iceland are dominantly kinetically-

424 limited (Dellinger et al., 2015; Gíslason et al., 1996). Instead, allophane is poorly crystalline

425   and can form rapidly in these soils, and together with ferrihydrite (which does not show a

426   useful correlation with δ^7Li), tends to dominate both the secondary weathering products and

427   the exchangeable components in these volcanic soils (i.e., in many Icelandic soils it is the

428   dominant silicate secondary mineral), especially at pH > 4.9 (Opfergelt et al., 2014;

429   Sigfússon et al., 2008). As mentioned above, the similar trend in δ^7Li_{soil} with allophane

430   contents is then likely caused by allophane precipitating from isotopically heavy pore waters.

431   Formation from the congruent dissolution of volcanic ash is unlikely, because measured ash

432   has a δ^7Li lower than that of the heaviest soils (Pogge von Strandmann et al., 2012). This

433   requires that allophane precipitating from the very first step of dissolution (when solution

434   δ^7Li would presumably be close to primary rock δ^7Li) is not resolved in this study – either

435   because it is not present (unlikely, given that allophane is the first silicate secondary mineral

436   to form in Iceland (Arnalds, 2004)), or more likely that it is not resolvable in bulk soils due to

437   mass balance. A mass balance, using the fractionation factor determined below and a basaltic

438   starting composition, suggests that the first 20% of Li transferred from solution to secondary

439   minerals would have a δ^7Li <0‰, and the total δ^7Li of the solid after taking up 60% of Li

440   from solution would be +1‰. The calculations below (Section 5.4) show that, on average, 80

441   ± 27% of Li is removed from solution, which would yield a clay δ^7Li of 2.5‰, if starting

442   from congruent basaltic dissolution. In other words, the initial light precipitated solid is not

443   detectable in bulk measurements.

444   It therefore appears likely that the Li isotope composition of the pore waters is

445   largely being controlled by the formation of the more rapidly forming poorly crystalline

446   allophane, rather than the slower formation of crystalline clays such as smectite or kaolinite,

447   which are only detectable in the HA soil by XRD (Opfergelt et al., 2014). The clay fraction is

448   comprised of the <2μm fraction, so includes Fe-oxyhydroxides as well as clays. However,

449   there is no co-variation between pore water δ^7Li and Fe extracted by dithionite-citrate-

450   bicarbonate (DCB) (Opfergelt et al., 2017b), suggesting that neither crystalline clays nor Fe-

451   oxyhydroxides are controlling Li isotopes here.

452   The relatively low pH of the poorly-drained H and HA pore waters also results in a

453   co-variation between δ^7Li_{PW} and pH (Fig. 8d). Primary silicate dissolution will consume

454   protons, raising pH. In contrast, secondary mineral formation will tend to release protons,

455   thus lowering pH. Organic matter decomposition will also have the same effect (Gislason and

456   Eugster, 1987; Pogge von Strandmann et al., 2010), and in the peaty H and HA soils, it is

457   likely this latter process that is affecting pH. Thus, the soils with the highest clay-sized

458   contents have the lowest pore water pH, but this does not appear to be affecting the pore

459   water Li isotope ratio. Instead, the relationship is due to a positive co-variation between pH

460   and the saturation index of allophane. This agrees with the overall observation that allophane

461   only forms above pH 4.9 when Al stops forming a complex with humus (Mizota and van

462   Reeuwiik, 1989). This then provides further evidence that it is the formation of allophane

463   over other clays that is dominating Li isotope fractionation.

464

465   5.3.1 Using Li/Na ratios to constrain Li isotope fractionation factors

466   To further understand the processes controlling δ^7Li_{PW}, the isotope ratios can be

467   compared to the Li/Na ratios (Liu et al., 2015). In these pore waters, there is a strong negative

468   correlation between δ^7Li_{PW} and Li/Na* (Fig. 9), as would be expected if secondary minerals

469   take up Li over Na, and the lighter Li isotope preferentially. Similar relationships have been

470   seen in basaltic rivers from Iceland and elsewhere (Liu et al., 2015; Pogge von Strandmann et

471   al., 2010; Pogge von Strandmann et al., 2006; Pogge von Strandmann et al., 2016; Pogge von

472   Strandmann et al., 2017b; Vigier et al., 2009). The interesting feature concerning the

473   relationship observed here, however, is that the pore waters from the soils that have

474   undergone the most weathering (HA and H, as determined from CRB depletion) are the least

475   fractionated from basalt or bulk soils for both Li/Na and δ^7Li_{PW} (i.e. most congruent

476   dissolution), while those that have undergone the least weathering (BA and GA), and overall

477   have the lowest total clay-sized contents, are the most fractionated, implying that they also

478   have the most secondary mineral formation. In general, H and HA soils are more poorly

479   drained that BA or GA soils. In principle, that should lead to greater water-rock contact times

480   in the H and HA soils, which would promote secondary mineral formation and raise solution

481   δ^7Li (Dellinger et al., 2015; Pogge von Strandmann et al., 2017b; Pogge von Strandmann and

482   Henderson, 2015). Given that this is the opposite to what is observed, other processes must be

483   controlling the pore water δ^7Li composition.

484   Interestingly, both HA soil profiles (i.e., from this study and from Pogge von

485   Strandmann et al., 2012) plot along the same δ^7Li_{PW} vs. Li/Na trend (Fig. 9), suggesting that

486   while their isotope ratios are different, the fractionation factors are the same in both soils. In

487   other words, a different amount of Li has been removed from the water by secondary mineral

488   formation, but with the same fractionation factor. Hence, the pore waters imply that the Histic

489   Andosol from this study is dissolving almost congruently at the base of its profile (Fig. 9).

490   These are the O layers of the soil, and it may be that organic acids are driving the pH low,

491   and causing more congruent dissolution of primary and/or secondary minerals.

492   If allophane is dominating Li removal from the remaining pore waters, then it is

493   possible to calculate an isotopic fractionation factor, based on the removal of Li relative to Na

494   from solution. The logarithmic relationship between Li/Na and δ^7Li for the trend shown by

495   the GA, BA and HA pore waters can be modelled using a Rayleigh fractionation relationship.

496   The starting composition can either be set to the host soils (as in Fig. 9b), or the pristine

497   basalt. The two starting compositions make little overall difference to the fractionation factor

498   α, which varies by 0.01 according to the initial material. The average Rayleigh α value for

499   these soils is 0.993 ± 0.03 (Fig. 9b), identical to the average α value of 0.992 for all basaltic

500   rivers (Pogge von Strandmann et al., 2017b), and to the α value of 0.991 determined in

501   inorganic basalt-water weathering experiments (Pogge von Strandmann et al., 2019a).

502   Equilibrium fractionation factors are also shown in Figure 9b, but the trends of the data do

503   not appear to follow linear trends, except potentially for the HA pore waters. In general,

504   therefore, the similarity in fractionation factors between soils, inorganic experiments and

505   rivers argues that the overall fractionation of Li isotopes during basalt weathering is similar

506   regardless of first order controls, such as runoff or climate. These factors may however be the

507   cause of the scatter observed in global basaltic rivers. In addition, the similarly of the soil and

508   river fractionation factors with inorganic experiments suggests that vegetation does not form

509   a significant control on the Li isotope composition of surface waters, or that vegetation

510   imposes an identical fractionation factor.

511   In general, if most of the pore waters can be modelled by a similar fractionation

512   factor, it would supply strong evidence that one secondary mineral is dominantly removing Li

513   from solution (Hindshaw et al., 2019). In this case, given the co-variation with δ^7Li_{PW}, this

514   mineral would appear to be allophane, which also agrees with the similar values of the histic

515   andosol reported in Pogge von Strandmann et al. (2012), where allophane was also the

516   dominant silicate secondary mineral. The similar positive co-variation between bulk soil δ^7Li

517   and allophane contents could therefore also imply that the allophane is forming through

518   uptake of Li from the pore waters, driving the bulk soil Li isotope ratio heavy as well. In

519   effect, this could explain why the 'closed-system' relationship of Rayleigh fractionation

520   appears to fit the fractionation behaviour better than equilibrium fractionation. This would be

521   because allophane formation (or at least its uptake of Li) is faster than the residence time of

522   the pore waters, meaning that they behave as a closed system. This applies even to the

523   rapidly-draining BA and GA soils, suggesting that Li uptake is very rapid, and indeed water-

524   basalt interaction experiments show that solution δ^7Li shows more than 12‰ fractionation

525   within 12 days, and more than 16‰ in a month (Pogge von Strandmann et al., 2019a).

526

527   *5.4 Element mobility and co-variation with Li isotopes*

528   The use of Li isotopes as a palaeo-weathering tracer (Hathorne and James, 2006;

529   Pogge von Strandmann et al., 2017a) opens the discussion as to whether Li isotopes only

530   inform on weathering regime changes (Dellinger et al., 2015), or whether they can inform on

531   CO_2 drawdown efficiency (Pogge von Strandmann and Henderson, 2015). The latter requires

532   that Li isotopes can be used to determine behaviour of the critical elements to the carbon

533   cycle, calcium and magnesium. This can be examined through the mobility of elements,

534   which is the tendency of elements to stay in solution (= mobile) compared to that of going

535   into secondary minerals (=immobile) (Gíslason et al., 1996). This is determined by the ratio

536   of the elements in question (here, Li to Ca) of the dissolved load to that of a starting

537   composition (here, either parent basalt, or host soil). A relative mobility value of 1 implies

538   that the Li/Ca ratio of the water is the same as that of the starting material, while lower values

539   mean that Ca is more mobile than Li.

540   Icelandic rivers exhibit a very strong relationship between Li to Ca relative mobility

541   and their δ^7Li value ($r^2 = 0.7$; Fig. 10a), as well as a similar one for Li to Mg mobility ($r^2 =$

542   0.67; Fig. 10c) (Pogge von Strandmann et al., 2016; Pogge von Strandmann et al., 2020). In

543   turn, this means that Li isotopes ratios could inform on the sequestration efficiency of CO_2.

544   The soil pore waters exhibit a similar, albeit more scattered, relationship. The GA waters

545   have the lowest Li mobility (compared to Ca or Mg), and, given that the decrease in Li

546   mobility is due to uptake by secondary minerals, the highest δ^7Li_{PW}. The HA and H waters

547   show contrasting behaviour (Fig. 10a), with the HA waters having low δ^7Li_{PW} but still higher

548   Ca or Mg than Li mobility, while the H waters have intermediate δ^7Li_{PW}, but a greater Li

549   mobility than Ca.

550   When comparing the mobility vs. δ^7Li_{PW} trend of these pore waters to basaltic rivers

551   from Iceland (Pogge von Strandmann et al., 2006) and the Azores (Pogge von Strandmann et

552   al., 2010), as well as the other Icelandic Histic Andosol (Pogge von Strandmann et al., 2012),

553   the HA soils from this study lie off the overall trend. If they are removed from the overall

554   pore water trend, then that trend and its r^2 becomes similar to that for the rivers ($r^2 = 0.7$ for

555   Ca, Fig. 10a; $r^2 = 0.55$ for Mg, Fig. 10c).

556   The behaviour of the pore waters can be taken further: a simple Rayleigh relationship,

557   using the best-fit alpha value from Section 5.3.1, can be used to determine the fraction of Li

558   taken into solution (Pogge von Strandmann et al., 2012; Vigier et al., 2009)(Fig. 10b). Thus,

559   on average the GA pore waters have the lowest fraction of Li in solution (average $7 \pm 4\%$,

560   where the uncertainty stems from the uncertainty in α), which increases to averages of $9 \pm$

561   6% in the BA pore waters, $14 \pm 7\%$ in the H and $50 \pm 6\%$ in the HA (up to 97% in some HA

562   waters). Again, as above, excepting the HA pore waters, there is a significant ($p<0.01$,

563   Spearman Rank) relationship between the Li to Ca relative mobility (and Li to Mg relative

564   mobility) and δ^7Li_{PW}, or the fraction of Li in solution that is derived from the δ^7Li_{PW} value

565   (Fig. 10b and d). In effect, when ~10% total Li is in solution, then Li and Ca or Mg are

566   similarly mobile (relative mobility $\sim 1^{+1.5}_{-0.5}$). In contrast, where ~2% of total Li is in solution,

567   Li is approximately a factor of 50 times less mobile than Ca (relative mobility $\sim 0.02^{+0.06}_{-0.015}$),

568   due to uptake into secondary minerals. This type of relationship has been reported in

569   experimental basalt-water interactions (Pogge von Strandmann et al., 2019a), as well as in

570   basaltic, andesitic and gneissic rivers (Clergue et al., 2015; Pogge von Strandmann et al.,

571   2010; Pogge von Strandmann et al., 2006; Pogge von Strandmann et al., 2020; Wimpenny et

572   al., 2010), and suggests that the δ^7Li value can be used to both determine the fraction of Li in

573   solution (i.e. the weathering regime) and from that the behaviour of Ca in solution. This

574   would be interesting especially from a palaeo-weathering perspective (Misra and Froelich,

575   2012; Pogge von Strandmann et al., 2017a; Pogge von Strandmann et al., 2013), because it

576   implies that the behaviour of an element directly involved in sequestering CO_2 could be

577   quantified. However, the HA pore waters here exhibit a trend with a significantly different

578   gradient from the other samples (Fig. 10b and d), and this highlights that more characterising

579   work is necessary. In this case, as mentioned above, the HA pore waters appear to follow a

580   linear rather than log trend in δ^7Li vs. Li/Na space (Fig. 9), potentially suggesting equilibrium

581   fractionation, and hence a subtly different fractionation factor. This may be because there are

582   hints that other clays are forming in these soils, compared to the other profiles (Opfergelt et

583   al., 2014; Opfergelt et al., 2017a; Opfergelt et al., 2017b).

584

585   *5.5 Li vs. Mg isotopes*

586   Magnesium is a critical element in the carbon cycle, because of the formation of Mg-

587   carbonates that sequester CO_2, and the exchange of Mg for Ca at mid-ocean ridges

588   (Humphris and Thompson, 1978; Walker et al., 1981). Mg isotopes have been suggested as a

589   tracer of Mg behaviour, but the processes that control Mg isotopes are complex, and include

590   lithology, secondary minerals and plants (Hindshaw et al., 2020; Tipper et al., 2006a; Tipper

591   et al., 2006b). It may be possible to constrain weathering processes using a combination of

592   isotopic systems, including those of Li and Mg. In particular, because Li substitutes for Mg in

593   both primary and secondary silicates (Hindshaw et al., 2019). Magnesium isotopes from these

594   particular soils and pore waters have been interpreted as representing a combination of Mg

595   adsorption by the soil exchangeable fraction (of heavy Mg isotopes preferentially) and of Mg

596   uptake by vegetation (which also takes up heavy Mg isotopes preferentially) (Opfergelt et al.,

597   2014). A strong control on Mg isotopes by adsorption onto allophane has also been reported

598   in other Icelandic soils (Pogge von Strandmann et al., 2012). When plotted against Li

599   isotopes (Fig. 11a), the pore waters are always isotopically lighter than the host basalt and

600   soils for Mg isotopes, but (as mentioned above), some pore waters have similar isotope ratios

601   to their host soils for Li isotopes.

602   Excluding the largely unfractionated HA from this study (bearing in mind that the

603   Histic Andosol studied by Pogge von Strandmann et al. (2012) behaves slightly differently –

604   Fig. 11a), there is a general negative relationship between Li and Mg isotopes, largely due to

605   the preferential uptake and sorption of light Li and heavy Mg by secondary minerals. Hence,

606   although there is scatter in any potential relationship, it is interesting that the pore waters

607   from soils that are nominally the least weathered are the most fractionated for both Li and Mg

608   isotopes. This supports the hypothesis that the secondary mineral that is affecting the sampled

609   pore waters (or at least their Li and Mg behaviour) is allophane, rather than other clays that

610   take longer to form, because it is the most fractionated (least weathered) soils that yield the

611   most favourable chemical conditions for allophane formation.

612   However, it is also clear that there is significant scatter in the relationship for these

613   pore waters between Li and Mg isotopes (Fig. 11a). In the absence of Mg-rich secondary

614   minerals in these soils (Opfergelt et al., 2014; Pogge von Strandmann et al., 2012; Sigfússon

615   et al., 2006, 2008), both Li and Mg are controlled by incorporation by substitution and

616   adsorption. However, the substitution and especially the sorption kinetics are different for the

617   two elements (experimentally by a factor of ~2.6 (Pogge von Strandmann et al., 2021b)),

618   meaning that similar behaviour will decouple the two elements and their isotopes. Scatter is

619   also caused by Mg uptake by plants, which causes isotope fractionation, and in these soils is

620   thought to be an important controlling process for Mg isotope ratios (Opfergelt et al., 2014).

621   Thus, even in the relatively simple weathering environment of Iceland, elements and isotopic

622   systems that are coupled by the same overall process (silicate weathering) and decoupled by

623   the specifics of the process for each element.

624

625   *5.6 Li vs. Si isotopes*

626   Silicon is another critical element in the carbon cycle, largely because it is the

627   weathering of silicates that ultimately removes atmospheric CO_2, and also because Si can be

628   a critical nutrient in certain ocean environments (Frings et al., 2016; Hatton et al., 2019). Si

629   isotopes are often interpreted similarly to Li isotopes, because secondary minerals

630   preferentially take up the light Si isotopes, driving waters isotopically heavy, and because

631   both trace silicate weathering processes (De la Rocha et al., 2000; Georg et al., 2007).

632   Because of this, both isotope systems exhibit a general positive covariation when comparing

633   all global river and pore water data (Pogge von Strandmann et al., 2017b). However, some

634   studies, including from Iceland, have shown a significant degree of scatter between Li and Si

635   isotopes, taken to be either influenced by plants (which preferentially take up light Si

636   isotopes, but do not fractionate Li isotopes), or due to kinetic differences if Si is dominated

637   by neoformation, compared to faster incorporation or adsorption for Li isotopes (Georg et al.,

638   2007; Georg et al., 2009; Opfergelt et al., 2013; Pogge von Strandmann et al., 2006; Pogge

639   von Strandmann et al., 2019b; Pogge von Strandmann et al., 2012; Vigier et al., 2009).

640   In our data, all the soils are isotopically lighter than the host basalt for Si isotopes

641   (Fig. 11b), due to the formation of secondary minerals (Opfergelt et al., 2017b). In contrast,

642   soil δ^7Li of the present study is only occasionally lower than the value for basalt, and there is

643   no correlation between bulk soil δ^7Li and $\delta^{30}Si$ for any of the soil profiles. Given that

644   secondary minerals clearly do take up the light isotopes of both elements (because pore

645   waters are isotopically heavy), this behaviour may be a function of the overall mass balance.

646   Because Si makes up a significant portion of clays (for example, Si makes up 20 molar% of

647   forsterite, 28% of Ca-montmorillonite and 14% of allophane), but Li does not (at most 0.01%

648   of clays), the bulk soil $\delta^{30}Si$ will be measurably perturbed by clay formation, while the bulk

649   soil δ^7Li will largely not be.

650   In contrast, the pore waters are clearly affected by secondary mineral formation in

651   both systems, driving an overall positive co-variation between δ^7Li and $\delta^{30}Si$ (Fig. 11b).

652   However, this co-variation does not exist for individual soil profiles. Further, the pore waters

653   that are most fractionated for Li isotopes (GA and BA) are not for Si, where the heaviest

654   values are from the Histosol (and also the HA of Pogge von Strandmann et al., 2012). From

655   the relationship between δ^7Li and Li/Na discussed above (Fig. 11a), it is clear that the Li

656   isotopes in the pore waters are only being fractionated by a single process (or processes with

657   a uniform fractionation factor), which then suggests that more variable processes are

658   affecting the Si isotope ratios of the pore waters. These likely include uptake by plants, and

659   the varying (and generally slower) kinetics that can affect the uptake of a major element into

660   secondary minerals (Opfergelt et al., 2017b; Pogge von Strandmann et al., 2012).

661   The relationships between δ^7Li and Mg and Si isotopes indicate the differing and

662   multiple processes that control Mg and Si over those that control Li (given the virtually linear

663   relationship between δ^7Li and Li/Na). This therefore demonstrates the potential

664   complications that can affect major elements over trace elements with relatively simple

665   behaviour during weathering such as Li (Pogge von Strandmann et al., 2019b), and also

666   confirms the potential of Li isotopes as a weathering tracer.

667

668   <u>6.0 Conclusions</u>

669   This study has analysed Li isotope ratios from well-studied soil and pore water

670   profiles from Iceland that have experienced different amounts of chemical weathering. Pore

671   waters from the soils that have experienced least weathering, based on the total reserve in

672 bases (Gleyic Andosol and Brown Andosol) have the highest $\delta^7 Li_{PW}$ values (14–34‰), and

673 these soils are also enriched in Li compared to their parent basalts. In contrast, those that are

674 more weathered (HA and H) have the lowest $\delta^7 Li_{PW}$ values (-1.4–20‰), and the bulk soils

675 are depleted in Li.

676   The pore waters form a well-defined negative trend for $\delta^7 Li$ as a function of Li/Na

677 ratios, suggesting that they are controlled by a process with a single fractionation factor,

678 likely the formation of allophane. Hence, a large range of solution $\delta^7 Li$ (~36‰) can be

679 generated by weathering with a single fractionation factor, due to variable proportion of Li

680 uptake. The correlation between $\delta^7 Li$ and uptake presents the possibility of combining

681 isotope ratio and flux into a single solution when interpreting palaeo—records. The isotopic

682 fractionation does not correspond to the amount of clay-sized material present, but to the

683 amount of clay undergoing neoformation. In other words, it is secondary minerals that are

684 currently forming, rather those that have previously formed, which control the $\delta^7 Li$ of surface

685 waters. Hence, profiles that have experienced only little overall chemical weathering, but

686 have formed a relatively large amount of amorphous, rapidly-formed, secondary minerals

687 (allophane), can exhibit substantial Li isotope fractionation.

688   Most of the pore waters also plot along the same trend between $\delta^7 Li$ and the relative

689 mobility of Li to Ca or Li to Mg as other Icelandic surface waters. This suggests that

690 dissolved Li isotope ratios can be used not only to inform on Li behaviour and the silicate

691 weathering regime, but also Ca behaviour. Effectively, this can then be used to determine the

692 fraction of Ca in solution vs. secondary minerals in palaeo-records, and thus CO_2 drawdown

693 efficiency. In other words, with data from more weathering lithologies, Li isotopes may be

694 useful for quantitively determining past CO_2 drawdown behaviour.

695

696

702

703

704

705   Ameijeiras-Mariño, Y., Opfergelt, S., Schoonejans, J., Vanacker, V., Sonnet, P., de Jong, J.T.M.
706   and Delmelle, P. (2017) Impact of low denudation rates on soil chemical weathering
707   intensity: A multiproxy approach. Chem. Geol. 456, 72–84.
708   Arnalds, O. (2004) Volcanic soils of Iceland. Catena 56, 3-20.
709   Berner, R.A., Lasaga, A.C. and Garrels, R.M. (1983) The Carbonate-Silicate Geochemical Cycle
710   and Its Effect on Atmospheric Carbon-Dioxide over the Past 100 Million Years. Am. J. Sci.
711   283, 641-683.
712   Bouchez, J., von Blanckenburg, F. and Schuessler, J.A. (2013) Modeling novel stable isotope
713   ratios in the weathering zone. Am. J. Sci. 313.
714   Brimhall, G.H. and Dietrich, W.E. (1987) Constitutive mass balance relations between
715   chemical composition, volume, density, porosity, and strain in metasomatic hydrochemical
716   systems: results on weathering and pedogenesis. Geochim. Cosmochim. Acta 51, 567–587.
717   Chadwick, O.A., Brimhall, G.H. and Hendricks, D.M. (1990) From a black to a gray box – a
718   mass balance interpretation of pedogenesis. Geomorphology 3, 369–390.
719   Chan, L.H., Edmond, J.M., Thompson, G. and Gillis, K. (1992) Lithium isotopic composition of
720   submarine basalts: implications for the lithium cycle in the oceans. Earth Planet. Sci. Lett.
721   108, 151-160.
722   Clergue, C., Dellinger, M., Buss, H.L., Gaillardet, J., Benedetti, M.F. and Dessert, C. (2015)
723   Influence of atmospheric deposits and secondary minerals on Li isotopes budget in a highly
724   weathered catchment, Guadeloupe (Lesser Antilles). Chem. Geol. 414, 28–41.
725   De la Rocha, C.L., Brzezinski, M.A. and DeNiro, M.J. (2000) A first look at the distribution of
726   the stable isotopes of silicon in natural waters. Geochim. Cosmochim. Acta 64, 2467-2477.
727   Dellinger, M., Gaillardet, J., Bouchez, J., Calmels, D., Louvat, P., Dosseto, A., Gorge, C.,
728   Alanoca, L. and Maurice, L. (2015) Riverine Li isotope fractionation in the Amazon River
729   basin controlled by the weathering regimes. Geochim. Cosmochim. Acta 164, 71–93.
730   Delvaux, B., Herbillon, A.J. and Vielvoye, L. (1989) Characterization of a Weathering
731   Sequenceof Soils Derived from Volcanic Ash in Cameroon. Taxonomic, Mineralogical and
732   Agronomic Implications. Geoderma 45, 375–388.
733   Faure, G. (1986) Principles of Isotope Geology, 2nd ed. Wiley.
734   Frings, P.J., Clymans, W., Fontorbe, G., De la Rocha, C.L. and Conley, D.J. (2016) The
735   continental Si cycle and its impact on the ocean Si isotope budget. Chem. Geol. 425, 12–36.

736 Georg, R.B., Reynolds, B.C., West, A.J., Burton, K.W. and Halliday, A.N. (2007) Silicon isotope
737 variations accompanying basalt weathering in Iceland. Earth Planet. Sci. Lett. 261, 476-490.
738 Georg, R.B., West, A.J., Basu, A.R. and Halliday, A.N. (2009) Silicon fluxes and isotope
739 composition of direct groundwater discharge into the Bay of Bengal and the effect on the
740 global ocean silicon isotope budget. Earth Planet. Sci. Lett. 283, 67-74.
741 Gíslason, S.R., Arnorsson, S. and Armannsson, H. (1996) Chemical weathering of basalt in
742 southwest Iceland: Effects of runoff, age of rocks and vegetative/glacial cover. Am. J. Sci.
743 296, 837–907.
744 Gislason, S.R. and Eugster, H.P. (1987) Meteoric water-basalt interactions. II: A field study in
745 N.E. Iceland. Geochim. Cosmochim. Acta 51, 2841–2855.
746 Gislason, S.R., Oelkers, E.H., Eiriksdottir, E.S., Kardjilov, M.I., Gisladottir, G., Sigfusson, B.,
747 Snorrason, A., Elefsen, S., Hardardottir, J., Torssander, P. and Oskarsson, N. (2009) Direct
748 evidence of the feedback between climate and weathering. Earth Planet. Sci. Lett. 277, 213-
749 222.
750 Grimm, C., Martinez, R.E., Pokrovsky, O.S., Benning, L.G. and Oelkers, E.H. (2019)
751 Enhancement of cyanobacterial growth by riverine particulate material. Chem. Geol. 525,
752 143–167.
753 Hathorne, E.C. and James, R.H. (2006) Temporal record of lithium in seawater: a tracer for
754 silicate weathering? Earth Planet. Sci. Lett. 246, 393–406.
755 Hatton, J.E., Hendry, K.R., Hawkings, J.R., Wadham, J.L., Kohler, T.J., Stibal, M., Beaton, A.D.,
756 Bagshaw, E.A. and Telling, J. (2019) Investigation of subglacial weathering under the
757 Greenland Ice Sheet using silicon isotopes. Geochim. Cosmochim. Acta 247, 191–206.
758 Hawley, S.M., Pogge von Strandmann, P.A.E., Burton, K.W., Williams, H.M. and Gislason, S.R.
759 (2017) Continental weathering and terrestrial (oxyhydr)oxide export: Comparing glacial and
760 non-glacial catchments in Iceland. Chem. Geol. 462, 55–66.
761 Henriet, C., De Jaeger, N., Dorel, M., Opfergelt, S. and Delvaux, B. (2008) The reserve of
762 weatherable primary silicates impacts the accumulation of biogenic silicon in volcanic ash
763 soils. Biogeochemistry 90, 209–223.
764 Hindshaw, R.S., Tosca, R., Gout, T.L., Farnan, I., Tosca, N.J. and Tipper, E.T. (2019)
765 Experimental constraints on Li isotope fractionation during clay formation. Geochim.
766 Cosmochim. Acta 250, 219–237.
767 Hindshaw, R.S., Tosca, R., Tosca, N.J. and Tipper, E.T. (2020) Experimental constraints on Mg
768 isotope fractionation during clay formation: Implications for the global biogeochemical cycle
769 of Mg. Earth Planet. Sci. Lett. 531, 115980.
770 Huh, Y., Chan, L.H. and Edmond, J.M. (2001) Lithium isotopes as a probe of weathering
771 processes: Orinoco River. Earth Planet. Sci. Lett. 194, 189–199.
772 Humphris, S.E. and Thompson, G. (1978) Hydrothermal Alteration of Oceanic Basalts by
773 Seawater. Geochim. Cosmochim. Acta 42, 107-125.
774 Kennedy, M.J., Löhr, S.C., Fraser, S.A. and Baruch, E.T. (2014) Direct evidence for organic
775 carbon preservation as clay-organic nanocomposites in a Devonian black shale; from
776 deposition to diagenesis. Earth Planet. Sci. Lett. 388, 59–70.
777 Kennedy, M.J. and Wagner, T. (2011) Clay mineral continental amplifier for marine carbon
778 sequestration in a greenhouse ocean. Proceedings of the National Academy of Sciences 108,
779 9776–9781.
780 Kisakürek, B., James, R.H. and Harris, N.B.W. (2005) Li and δ^7Li in Himalayan rivers: Proxies
781 for silicate weathering? Earth Planet. Sci. Lett. 237, 387–401.

782 Lalonde, K., Mucci, A., Ouellet, A. and Gelinas, Y. (2012) Preservation of organic matter in
783 sediments promoted by iron. Nature 483, 198–200.
784 Lechler, M., Pogge von Strandmann, P.A.E., Jenkyns, H.C., Prosser, G. and Parente, M. (2015)
785 Lithium-isotope evidence for enhanced silicate weathering during OAE 1a (Early Aptian Selli
786 event). Earth Planet. Sci. Lett. 432, 210–222.
787 Lemarchand, E., Chabaux, F., Vigier, N., Millot, R. and Pierret, M.C. (2010) Lithium isotope
788 systematics in a forested granitic catchment (Strengbach, Vosges Mountains, France).
789 Geochim. Cosmochim. Acta 74, 4612-4628.
790 Li, W. and Liu, X.-M. (2020) Experimental investigation of lithium isotope fractionation
791 during kaolinite adsorption: Implications for chemical weathering. Geochim. Cosmochim.
792 Acta 284, 156–172.
793 Li, W., Liu, X.-M. and Chadwick, O.A. (2020) Lithium isotope behavior in Hawaiian regoliths:
794 Soil-atmosphere-biosphere exchanges. Geochim. Cosmochim. Acta 285, 175–192.
795 Liu, X.-L., Rudnick, R.L., McDonough, W.F. and Cummings, M.L. (2013) Influence of chemical
796 weathering on the composition of the continental crust: Insights from Li and Nd isotopes in
797 bauxite profiles developed on Columbia River Basalts. Geochim. Cosmochim. Acta 115, 73–
798 91.
799 Liu, X.-M., Wanner, C., Rudnick, R.L. and McDonough, W.F. (2015) Processes controlling δ^7Li
800 in rivers illuminated by study of streams and groundwaters draining basalts. Earth Planet.
801 Sci. Lett. 409, 212–224.
802 Maher, K. (2011) The role of fluid residence time and topographic scales in determining
803 chemical fluxes from landscapes. Earth Planet. Sci. Lett. 312, 48–58.
804 Marriott, C.S., Henderson, G.M., Crompton, R., Staubwasser, M. and Shaw, S. (2004) Effect
805 of mineralogy, salinity, and temperature on Li/Ca and Li isotope composition of calcium
806 carbonate. Chem. Geol. 212, 5–15.
807 Millot, R., Vigier, N. and Gaillardet, J. (2010) Behaviour of lithium and its isotopes during
808 weathering in the Mackenzie Basin, Canada. Geochim. Cosmochim. Acta 74, 3897–3912.
809 Misra, S. and Froelich, P.N. (2012) Lithium Isotope History of Cenozoic Seawater: Changes in
810 Silicate Weathering and Reverse Weathering. Science 335, 818–823.
811 Mizota, C. and van Reeuwiik, L.P. (1989) Clay Mineralogy and Chemistry of Soils Formed in
812 Volcanic Material in Diverse Climatic Regions. Soil Monograph, ISRIC, Wageningen.
813 Opfergelt, S., Burton, K.W., Georg, R.B., West, A.J., Guicharnaud, R.A., Sigfusson, B., Siebert,
814 C., Gislason, S.R. and Halliday, A.N. (2014) Magnesium retention on the soil exchange
815 complex controlling Mg isotope variations in soils, soil solutions and vegetation in volcanic
816 soils, Iceland. Geochim. Cosmochim. Acta 125, 110–130.
817 Opfergelt, S., Burton, K.W., Pogge von Strandmann, P.A.E., Gislason, S.R. and Halliday, A.N.
818 (2013) Riverine silicon isotope variations in glaciated basaltic terrains: Implications for the Si
819 delivery to the ocean over glacial–interglacial intervals. Earth Planet. Sci. Lett. 369–370,
820 211–219.
821 Opfergelt, S., Cornelis, J.T., Houben, D., Givron, C., Burton, K.W. and Mattielli, N. (2017a)
822 The influence of weathering and soil organic matter on Zn isotopes in soils. Chem. Geol. 466,
823 140–148.
824 Opfergelt, S., Williams, H.M., Cornelis, J.T., Guicharnaud, R.A., Georg, R.B., Siebert, C.,
825 Gislason, S.R., Halliday, A.N. and Burton, K.W. (2017b) Iron and silicon isotope behaviour
826 accompanying weathering in Icelandic soils, and the implications for iron export from
827 peatlands. Geochim. Cosmochim. Acta 217, 273–291.

828   Penniston-Dorland, S., Liu, X.-M. and Rudnick, R.L. (2017) Lithium Isotope Geochemistry,
829   Rev. Min. Geochem., pp. 165–217.
830   Pistiner, J.S. and Henderson, G.M. (2003) Lithium-isotope fractionation during continental
831   weathering processes. Earth Planet. Sci. Lett. 214, 327-339.
832   Pogge von Strandmann, P.A.E., Burton, K.W., James, R.H., van Calsteren, P. and Gislason,
833   S.R. (2010) Assessing the role of climate on uranium and lithium isotope behaviour in rivers
834   draining a basaltic terrain. Chem. Geol. 270, 227–239.
835   Pogge von Strandmann, P.A.E., Burton, K.W., James, R.H., van Calsteren, P., Gislason, S.R.
836   and Mokadem, F. (2006) Riverine behaviour of uranium and lithium isotopes in an actively
837   glaciated basaltic terrain. Earth Planet. Sci. Lett. 251, 134–147.
838   Pogge von Strandmann, P.A.E., Burton, K.W., Opfergelt, S., Eiriksdottir, E.S., Murphy, M.J.,
839   Einarsson, A. and Gislason, S.R. (2016) The effect of hydrothermal spring weathering
840   processes and primary productivity on lithium isotopes: Lake Myvatn, Iceland. Chem. Geol.
841   445, 4–13.
842   Pogge von Strandmann, P.A.E., Dellinger, M. and West, A.J. (2021a) Lithium Isotopes: A
843   Tracer of Past and Present Silicate Weathering. Cambridge University Press.
844   Pogge von Strandmann, P.A.E., Desrochers, A., Murphy, M.J., Finlay, A.J., Selby, D. and
845   Lenton, T.M. (2017a) Global climate stabilisation by chemical weathering during the
846   Hirnantian glaciation. GPL 3, 230–237.
847   Pogge von Strandmann, P.A.E., Elliott, T., Marschall, H.R., Coath, C., Lai, Y.J., Jeffcoate, A.B.
848   and Ionov, D.A. (2011) Variations of Li and Mg isotope ratios in bulk chondrites and mantle
849   xenoliths. Geochim. Cosmochim. Acta 75, 5247–5268.
850   Pogge von Strandmann, P.A.E., Fraser, W.T., Hammond, S.J., Tarbuck, G., Wood, I.G.,
851   Oelkers, E.H. and Murphy, M.J. (2019a) Experimental determination of Li isotope behaviour
852   during basalt weathering. Chem. Geol. 517, 34–43.
853   Pogge von Strandmann, P.A.E., Frings, P.J. and Murphy, M.J. (2017b) Lithium isotope
854   behaviour during weathering in the Ganges Alluvial Plain. Geochim. Cosmochim. Acta 198,
855   17–31.
856   Pogge von Strandmann, P.A.E. and Henderson, G.M. (2015) The Li isotope response to
857   mountain uplift. Geology 43, 67–70.
858   Pogge von Strandmann, P.A.E., Hendry, K.R., Hatton, J.E. and Robinson, L.F. (2019b) The
859   Response of Magnesium, Silicon, and Calcium Isotopes to Rapidly Uplifting and Weathering
860   Terrains: South Island, New Zealand. Frontiers in Earth Science 7.
861   Pogge von Strandmann, P.A.E., James, R.H., van Calsteren, P., Gíslason, S.R. and Burton,
862   K.W. (2008) Lithium, magnesium and uranium isotope behaviour in the estuarine
863   environment of basaltic islands. Earth Planet. Sci. Lett. 274, 462-471.
864   Pogge von Strandmann, P.A.E., Jenkyns, H.C. and Woodfine, R.G. (2013) Lithium isotope
865   evidence for enhanced weathering during Oceanic Anoxic Event 2. Nature Geoscience 6,
866   668–672.
867   Pogge von Strandmann, P.A.E., Kasemann, S.A. and Wimpenny, J.B. (2020) Lithium and
868   Lithium Isotopes in Earth's Surface Cycles. Elements 16, 253–258.
869   Pogge von Strandmann, P.A.E., Opfergelt, S., Lai, Y.J., Sigfusson, B., Gislason, S.R. and
870   Burton, K.W. (2012) Lithium, magnesium and silicon isotope behaviour accompanying
871   weathering in a basaltic soil and pore water profile in Iceland. Earth Planet. Sci. Lett. 339–
872   340, 11–23.

Pogge von Strandmann, P.A.E., Renforth, P., West, A.J., Murphy, M.J., Luu, T.-H. and Henderson, G.M. (2021b) The lithium and magnesium isotope signature of olivine dissolution in soil experiments. Chem. Geol. 560, 120008.

Raymo, M.E. and Ruddiman, W.F. (1992) Tectonic Forcing of Late Cenozoic Climate. Nature 359, 117-122.

Revels, B.N., Rickli, J., Moura, C.A.V. and Vance, D. (2021) Nickel and its isotopes in the Amazon Basin: The impact of the weathering regime and delivery to the oceans. Geochim. Cosmochim. Acta 293, 344–364.

Ryan, J.G. and Kyle, P.R. (2004) Lithium abundance and lithium isotope variations in mantle sources: insights from intraplate volcanic rocks from Ross Island and Marie Byrd Land (Antarctica) and other oceanic islands. Chem. Geol. 212, 125–142.

Ryu, J.-S., Vigier, N., Lee, S.-W., Lee, K.-S. and Chadwick, O.A. (2014) Variation of lithium isotope geochemistry during basalt weathering and secondary mineral transformations in Hawaii. Geochim. Cosmochim. Acta 145, 103–115.

Sigfússon, B., Gislason, S.R. and Paton, G.I. (2006) The effect of soil solution chemistry on the weathering rate of a Histic Andosol. Journal of Geochemical Exploration 88, 321-324.

Sigfússon, B., Gislason, S.R. and Paton, G.I. (2008) Pedogenesis and weathering rates of a Histic Andosol in Iceland: Field and experimental soil solution study. Geoderma 144, 572-592.

Stefansson, A. and Gislason, S.R. (2001) Chemical weathering of basalts, Southwest Iceland: Effect of rock crystallinity and secondary minerals on chemical fluxes to the ocean. Am. J. Sci. 301, 513-556.

Steinhoefel, G., Brantley, S.L. and Fantle, M.S. (2021) Lithium isotopic fractionation during weathering and erosion of shale. Geochim. Cosmochim. Acta 295, 155–177.

Teng, F.Z., Li, W.Y., Rudnick, R.L. and Gardner, L.R. (2010) Contrasting lithium and magnesium isotope fractionation during continental weathering. Earth Planet. Sci. Lett. 300, 63-71.

Tessier, A., Campbell, P.G.C. and Bisson, M. (1979) Sequential Extraction Procedure for the Speciation of Particulate Trace Metals. Analytical Chemistry 51, 844-851.

Tipper, E.T., Galy, A. and Bickle, M.J. (2006a) Riverine evidence for a fractionated reservoir of Ca and Mg on the continents: Implications for the oceanic Ca cycle. Earth Planet. Sci. Lett. 247, 267-279.

Tipper, E.T., Galy, A., Gaillardet, J., Bickle, M.J., Elderfield, H. and Carder, E.A. (2006b) The magnesium isotope budget of the modern ocean: Constraints from riverine magnesium isotope ratios. Earth Planet. Sci. Lett. 250, 241-253.

Verney-Carron, A., Vigier, N., Millot, R. and Hardarsson, B.S. (2015) Lithium isotopes in hydrothermally altered basalts from Hengill (SW Iceland). Earth Planet. Sci. Lett. 411, 62–71.

Vigier, N., Decarreau, A., Millot, R., Carignan, J., Petit, S. and France-Lanord, C. (2008) Quantifying Li isotope fractionation during smectite formation and implications for the Li cycle. Geochim. Cosmochim. Acta 72, 780–792.

Vigier, N., Gislason, S.R., Burton, K.W., Millot, R. and Mokadem, F. (2009) The relationship between riverine lithium isotope composition and silicate weathering rates in Iceland. Earth Planet. Sci. Lett. 287, 434–441.

Wada, K., Arnalds, O., Kakuto, Y., Wilding, L.P. and Hallmark, C.T. (1992) Clay minerals of four soils formed in eolian and tephra materials in Iceland. Geoderma 52, 351-365.

918 Walker, J.C.G., Hays, P.B. and Kasting, J.F. (1981) A Negative Feedback Mechanism for the
919 Long-Term Stabilization of Earths Surface-Temperature. Journal of Geophysical Research-
920 Oceans and Atmospheres 86, 9776-9782.
921 West, A.J., Galy, A. and Bickle, M. (2005) Tectonic and climatic controls on silicate
922 weathering. Earth Planet. Sci. Lett. 235, 211–228.
923 Wimpenny, J., James, R.H., Burton, K.W., Gannoun, A., Mokadem, F. and Gislason, S.R.
924 (2010) Glacial effects on weathering processes: New insights from the elemental and lithium
925 isotopic composition of West Greenland rivers Earth Planet. Sci. Lett. 290, 427-437.

926

927

928

929

930

931

932

933

934

935

936

937

938

Bulk soils Soil name	ID	Horizon	Depth (cm)	C %	CEC cmolc.kg-1	TRB cmolc.kg-1	Ferrihydrite %	Allophane %	Total clay %	Na g/kg	Al g/kg	Fe g/kg	Ca g/kg	Mg g/kg	Zr µg/g	Li µg/g	δ⁷Li ‰	2sd
Histic Andosol	HA	A1	0-15	18.5	40.1	148	7.1	4.9	56.1	4.3	50.5	165.7	14.6	6.4	167	4.70	0.9	0.3
		A2	15-26	16.9	55.3	177	5.4	9.5	54.3	5.5	72	98.9	17.7	7.3	237	5.80	-0.3	0.2
		Bw1	26-40	14.5	61.8	138	11.9	8.3	55.2	4.4	60.4	175.1	13.8	5.6	201	4.60	1.4	0.3
		Bw2	40-57	16.9	53.8	156	7.1	6.9	45.5	6.5	63	164.4	16.1	5.0	263	4.53	-0.7	0.4
		O1	57-67	28.7	59.4	103	4.4	6.6	53.8	3.3	44	55.7	11	3.9	275	2.36	-0.8	0.3
		redox	67-83	12.8	28.3	332	1.4	6.9		18.7	78.6	57.6	30.2	9.9	431	11.0	3.0	0.2
		O2	83+	42.7	71.3	52.4	3.2	1.4	55.3	2.1	22.3	42.9	5.4	1.7	280	3.21	0.3	0.5
Histosol	H	O1	0-13	21.0	49.5	266	6.8	2.5	52.3	6.4	39.5	120.3	28.5	11.1	112	7.86	-1.1	0.2
		O2	13-26	22.9	39.5	192	3.8	1.8	8.4	5.6	37	83.8	19.2	8.1	131	6.30	-4.3	0.3
		O3	26-40	18.6	52.6	188	5.9	6.7	38.2	7.5	56.4	141.7	18.6	6.8	252	4.32	0.3	0.3
		T	40-52	12.0	43.2	60.9	43.5	9.8		1.2	20.9	341.5	7.6	2.1	74	0.83	6.9	0.5
		O4	52-63	10.3	30.0	283	3.3	4.6	44.4	15.1	63.4	101.6	26.4	8.6	339	10.3	-0.7	0.4
		O5	63-72	29.3	65.6	115	4.7	2.3	70.9	2.8	34.3	140.7	12.6	4.6	132	2.04	0.0	0.3
		O6	72+	30.4	85.3	118	3.9	3.5	42.7	3.6	35.5	86.6	12.7	4.4	212	4.54	-2.2	0.2
Brown Andosol	BA	A1	0-21	7.29	36.8	403	7.8	10.7	33.2	10	83.2	111.9	39.1	19.2	223	9.05	6.4	0.5
		A2	21-40	7.92	35.2	370	8.6	11.0	29.7	9.6	86.8	117.2	36.1	17.2	241	8.97	5.0	0.4
		Bw1	40-52	6.47	36.8	377	7.3	9.2	37.2	10.1	91.3	122.7	35.7	17.8	217	9.66	3.9	0.2
		Bw2	52-96	7.25	50.9	317	9.7	13.0	41.0	8.5	97	126.1	31.1	14.5	262	9.08	3.7	0.2
		Bw3/C	96+	5.71	42.7	324	8.5	12.6		9.8	94.4	127.9	31.5	14.1	246	11.8	2.1	0.4
Gleyic Andosol	GA	A1	0-12	9.51	47.0	333	7.4	9.8	37.1	7.3	84.1	104.5	30.7	17.3	191	8.94	5.6	0.3
		A2	12-29	6.20	46.5	377	8.5	12.2	41.2	7.7	85.1	119.2	35	19.7	218	10.3	5.1	0.3
		Bw1	29-43	6.86	46.7	275	6.4	14.7	38.9	7.3	91	116.7	27.5	12.2	250	10.3	6.6	0.4
		Bw2	43-56	6.76	49.9	293	4.6	15.4	36.3	7.6	93.6	105.5	29.7	12.8	262	11.0	5.0	0.3
		C	56-64	2.70	23.5	649	4.0	7.4		10.3	78.3	119.2	38	38	144	8.92	6.3	0.3
		2Bw1	64+	3.26	40.2	480	1.8	21.1	22.9	8.5	112.5	59.2	22.5	22.5	196	16.6	5.3	0.3
Vitrisol	V	A	0-9	0.32	13.2	667	3.9	8.9	4.6				61.5	32.0	235	10.8	2.1	0.5
		B/C	9-33	0.26	32.7	568	7.1	14.2	4.6				53	27.9	219	9.08	3.6	0.3
		C	33+		8.87										137	4.98	-0.2	0.1
Parental basalt										20.6	72.6	103.8	74	32.1	164	5.89	3.6	0.3

Secondary minerals	ID									Na	Al	Fe	Ca	Mg	Zr	Li	δ⁷Li	2sd
Calcite	Iceland spar									0.38	0.02	0.009	336	0.01				
Calcite	11551									0.30	0.03	0.003	346	3.32		0.04	0.4	0.6
Calcite	11547									0.29	0.05	0.028	358	3.77		0.03	-1.0	0.5
Calcite	7869									0.33	0.39	0.133	363	0.19		0.04	5.4	0.5
Clay	11571									0.40	83.6	292	6.10	55.7		13.4	-8.4	0.2
Clay	21637									3.38	55.2	109	11.8	16.7		5.35	2.1	0.2
Heulandite	11607									9.52	68.1	0.010	29.5	0.05		0.83	7.9	0.3
Chabazite	15227									6.07	89.7	0.12	49.5	0.07		1.00	-0.2	0.2
Mesolite	21633									29.0	139.5	1.17	72.4	0.75		2.29	-4.9	0.2
Stilbite	11933									11.9	72.1	7.60	36.8	2.88		2.09	-1.8	0.1
Epistilbite	11613									11.9	97.9	0.057	57.2	0.03		2.57	-1.0	0.3
Scolecite	4221									16.8	102	0.060	43.1	0.02		2.33	5.3	0.6
Fe-oxyhydroxide	A6									11.0	110	283	55.6	27.7		14.1		

Leaches (% Li of total)	Exchangeable	Carbonate	Oxide	Residue
HA 01	1.4	3.2	25.6	69.9
H O6	3.4	4.0	20.6	72.0
BA BW2	0.2	0.9	9.8	89.1

940 Table 1. Bulk soil and secondary mineral data. All soil data aside from Li isotope ratios are

941 from Opfergelt et al., 2014. The final section shows the results for Li from sequential

942 leaching of three soils.

943

944

945

Pore waters	Depth cm	pH	T °C	Li ng/ml	Na µg/ml	Mg µg/ml	Al ng/ml	K µg/ml	Ca µg/ml	Si µg/ml	Fe ng/ml	Cl µg/ml	δ^7Li ‰	2sd
2009														
HA H1	7.5	6.18	11.6	0.61	16.5	5.19	185	5.64	5.86	8.37	40.4	34.0	15.5	0.3
HA O1	62	3.64	11	3.02	7.87	3.60	10200	0.116	30.1	31.1	115	11	2.1	0.1
HA O2	83	3.71	10.9	3.02	8.95	3.56	9670	0.127	24.4	30.8	122	12	-1.4	0.2
H O1	6.5	4.34	11.3	4.17	9.17	4.16	316	0.390	9.88	17.40	13.8	9.0	14.6	0.5
H O5	67.5	4.78	11.7	3.02	16.1	3.33	15.8	0.318	4.29	13.90	519	22	14.3	0.3
H O6	72	5.48	11.6	5.94	19.6	10.9	90.8	0.746	11.2	18.3	25000	21	10.7	0.4
BA BW1	46	5.83	11.9	0.04	7.26	0.73	90.2	0.036	1.64	0.74	65.8	14.2	34.2	0.1
GA A1	6	5.64	13.1	0.12	7.83	1.46	106	0.326	3.78	4.89	38.6	25.9	28.5	0.3
GA BW1	36	5.90	13	0.08	7.53	1.20	9.6	0.041	3.54	7.95		13.6	34.2	0.2
GA 2BW1	64	5.88	12.9	0.08	6.93	2.00	11.6	0.011	5.94	13.80		12.1	29.5	0.4
2010														
HA H1	7.5	5.05	19.6	0.61	12.6	8.64	320	3.32	11.3	9.60	26.5	7.9	12.3	0.4
HA BW1	33	4.67	20.3	0.71	8.29	3.67	475	0.089	16.2	9.60	22.8	12.1	15.1	0.3
HA O1	62	3.99	18.9	1.80	6.70	4.13	6510	0.088	27.8	24.2	32.3	10.0	7.4	0.1
HA redox	75	3.98	18.5	2.97	8.54	3.60	7530	0.128	23.2	26.5	36.2	11.3	0.8	0.2
HA O2	83	3.95	18.3	2.80	9.52	4.34	7640	0.078	24.5	30.3	36.5	13.0	0.8	0.4
H O1	6.5	4.88	22.3	2.86	9.91	4.68	54.3	3.13	7.20	10.5	282	4	19.7	0.3
H O2	19.5	5.47	20.3	0.79	12.0	6.38	23.8	0.439	7.26	5.30	58.5	28.7	18.4	0.4
H O3	33	5.15	19.2	1.95	14.7	4.53	205	0.315	8.94	17.4	193	23	11.7	0.3
H O4	57.5			3.27	21.0	6.12	101	0.788	7.14	19.2	15300		14.1	0.6
H O6	72			7.48	25.4	17.1	45.7	1.72	15.2	18.8	20000		11.3	0.4
BA A1	10.5			0.06	6.38	1.51	4.93	1.23	2.13	5.90	12.1		28.4	0.6
BA A2	30.5	5.84	19.1	0.14	5.18	0.74	3.54	0.063	1.11	3.50	9.86	9.60	18.6	0.3
BA BW1	46	5.88	19	0.25	6.89	0.93	50.8	0.043	1.55	3.60	34.5	13.5	13.7	0.3
BA BW2	74	5.96	19.1	0.14	7.22	0.74	4.61	0.040	1.52	4.40	8.03	15.50	18.4	0.4
BA BW3	96	5.46	20	0.14	8.05	0.92	1.57	0.101	1.80	5.00	3.51	14.20	20.5	0.2
GA A1	6			0.05	6.87	1.79	17.3	2.318	3.75	5.70	13.6		31.6	0.4
GA A2	20.5	5.77	17.8	0.12	6.69	0.68	28.2	0.995	1.55	7.50	45.4	6.6	24.3	0.2
GA BW2	36			0.09	6.65	0.68	5.69	0.173	1.76	8.10	14.7		27.0	0.5
GA BW2	49.5	5.6	17.4	0.10	8.28	1.27	40.0	0.280	3.75	12.0	11.3	8.5	22.1	0.2
GA 2BW1	64	5.46	17.2	0.08	11.3	2.48	10.4	0.368	7.14	12.4	4.96	9.30	25.6	0.2

947   Table 2. Pore water data. All data aside from Li isotope ratios are from Opfergelt et al., 2014.
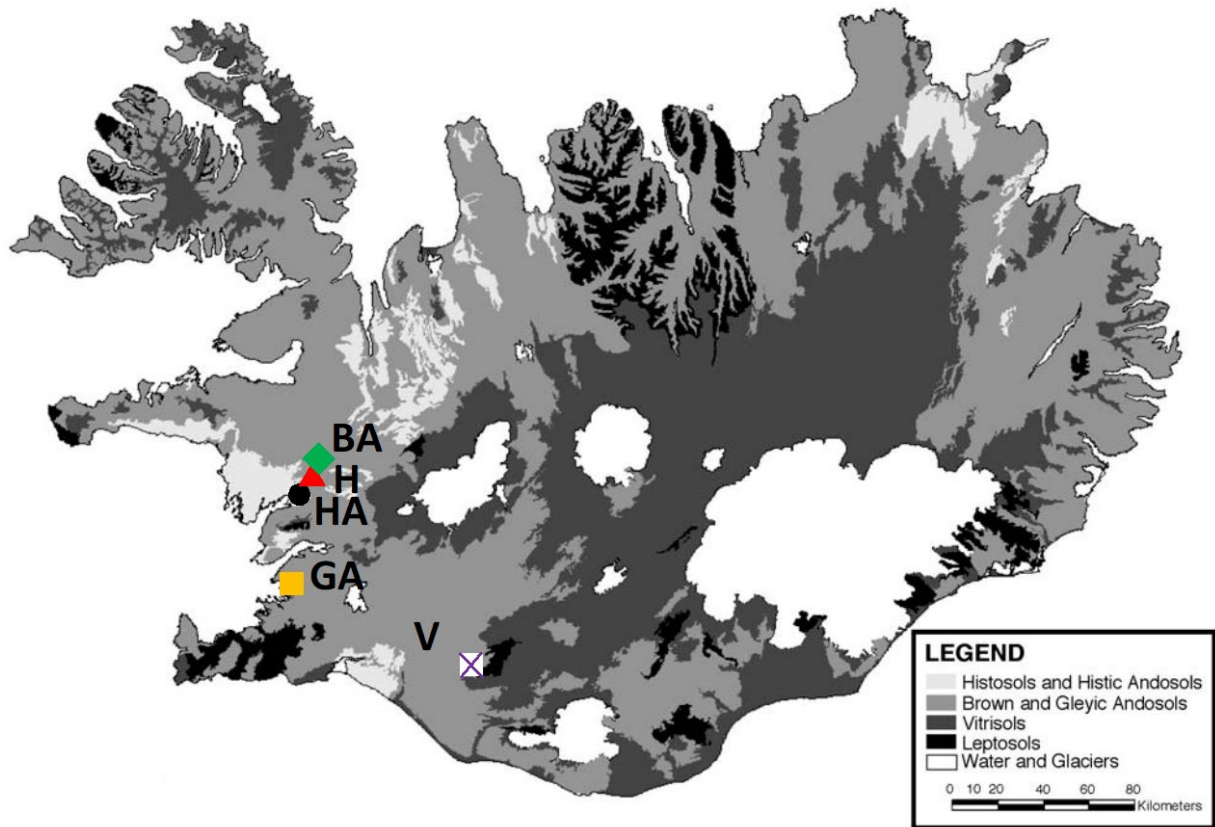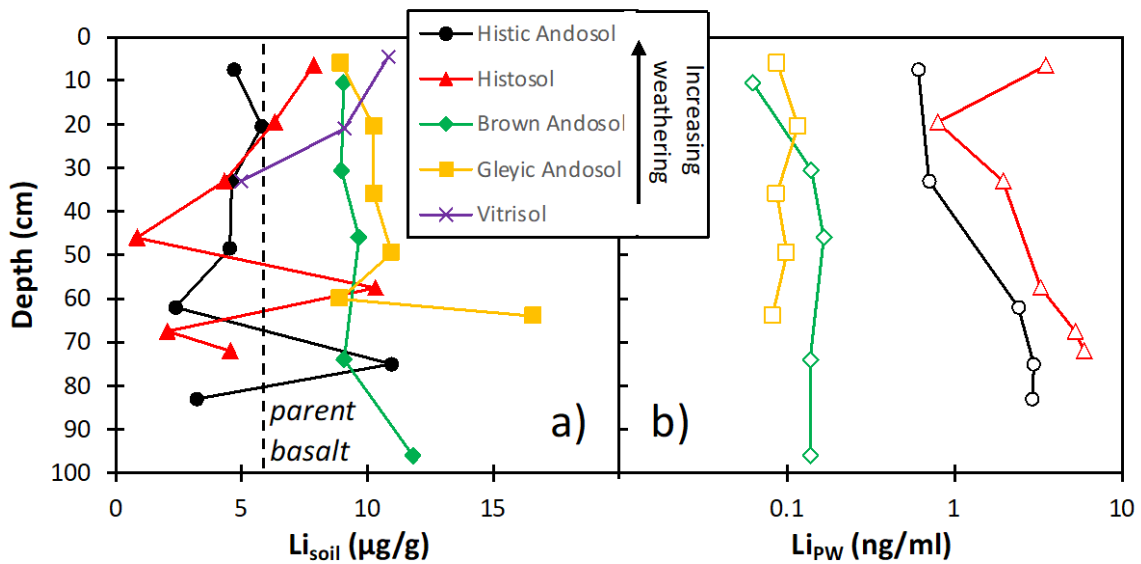
948

949

950

951

952

953

955   Figure 1. Sample locations on a soil map of Iceland. Soil symbols correspond to the key of

956   Figure 2. Adapted from Opfergelt et al., 2014.

Figure 2. Depth profiles for Li concentrations for bulk soils and parent basalt depicted by the

vertical dashed line (a), and pore waters (b). The pore water concentrations have been

averaged from the two different collection years for this diagram (Table 2).
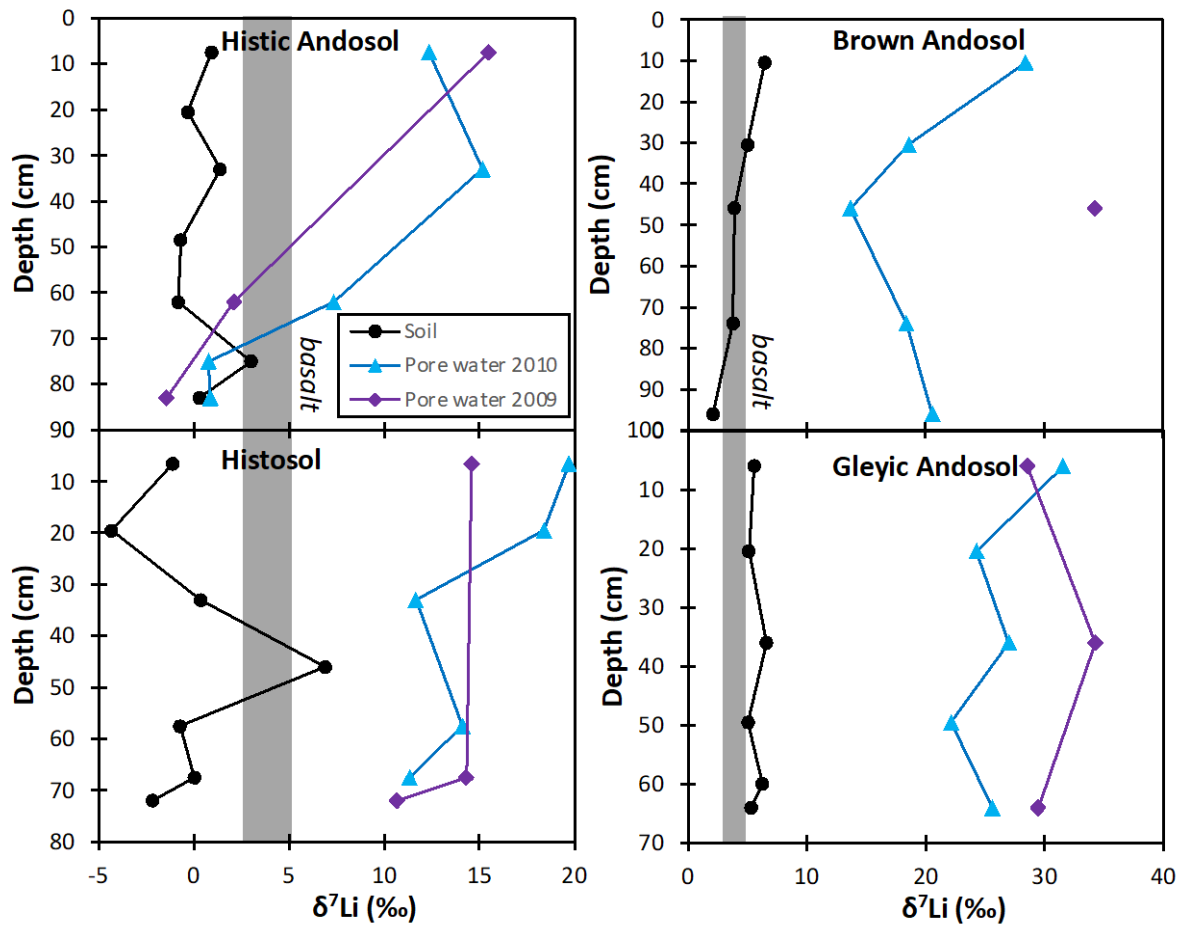
Figure 3. Li isotope depth profiles for bulk soils, and the two different seasons of pore waters.

In 2009, samples were taken in September (late summer), while in June (late spring) in 2010.

The range of Icelandic basalt is depicted by the shaded area. Note the difference in horizontal

axis scales.
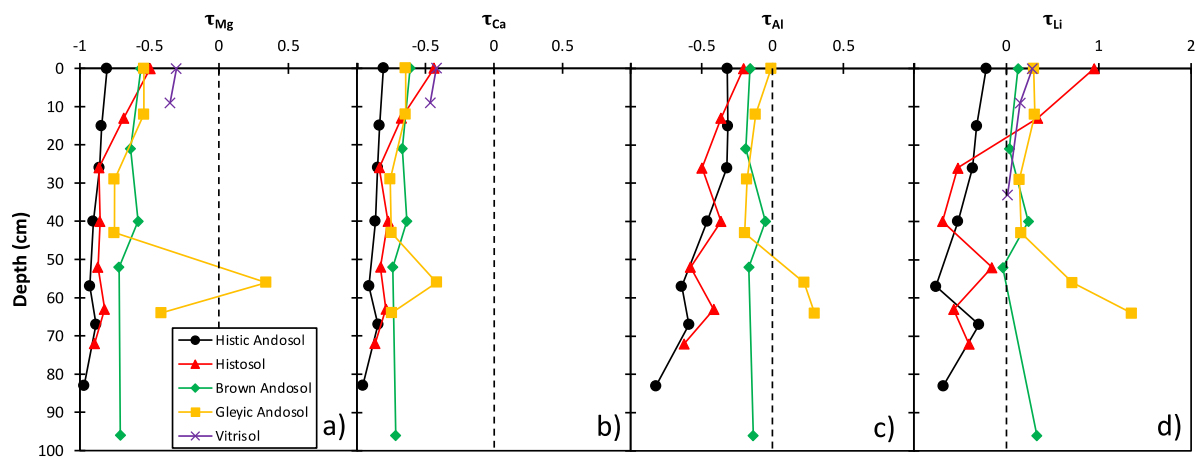
Figure 4. Tau values for the soils for the elements Mg, Ca, Al and Li. The dashed vertical lines are at tau = 0.
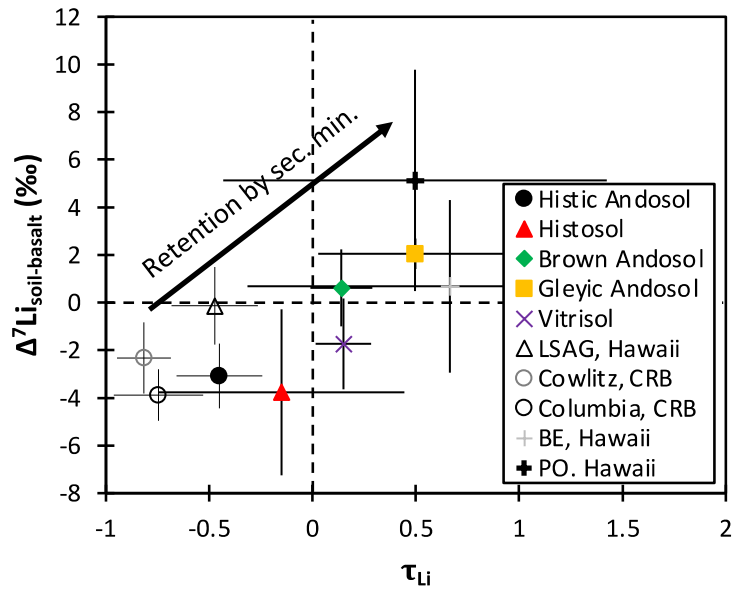
Figure 5. Average τ_{Li} and $\Delta^7 Li_{soil-basalt}$ values for each soil profile. The error bars represent the 1sd spread in the data. Also shown are data from the Columbia River Basalts (Liu et al., 2013) and multiple sections from Hawaii (Li et al., 2020; Ryu et al., 2014). Due to high aeolian input, the topsoil from Li et al. (2020) has been removed from the averages.

984

985

986

987

988

989

990

991

992
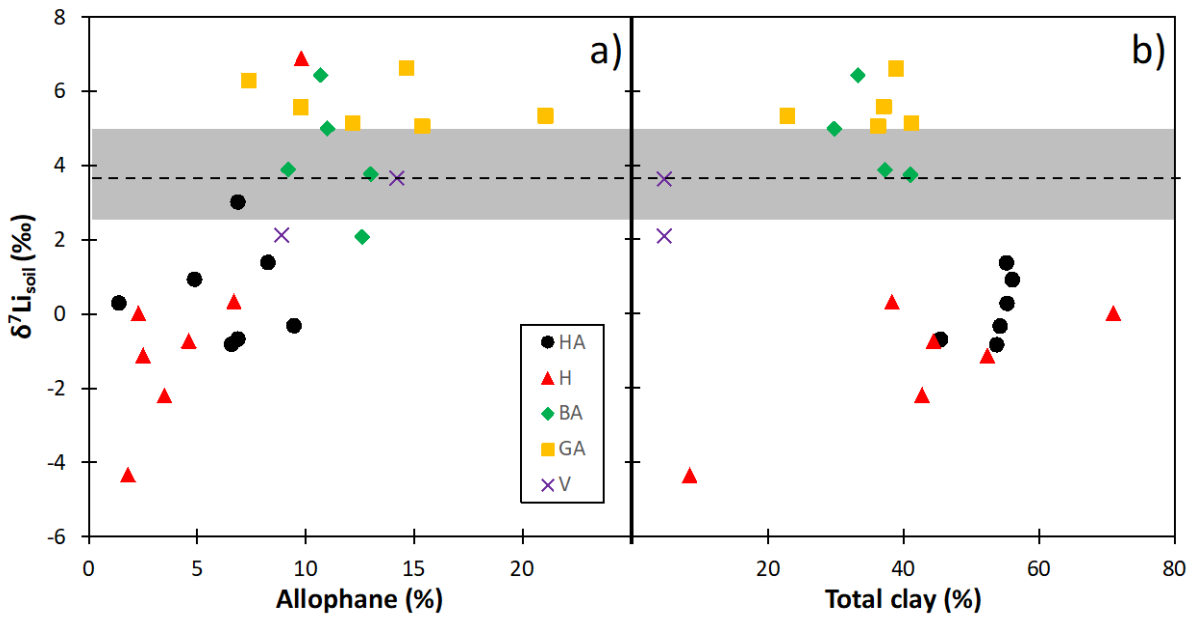
Figure 6. Bulk soil Li isotopes as a function of allophane content (a) and total clay-sized content (b).

1010
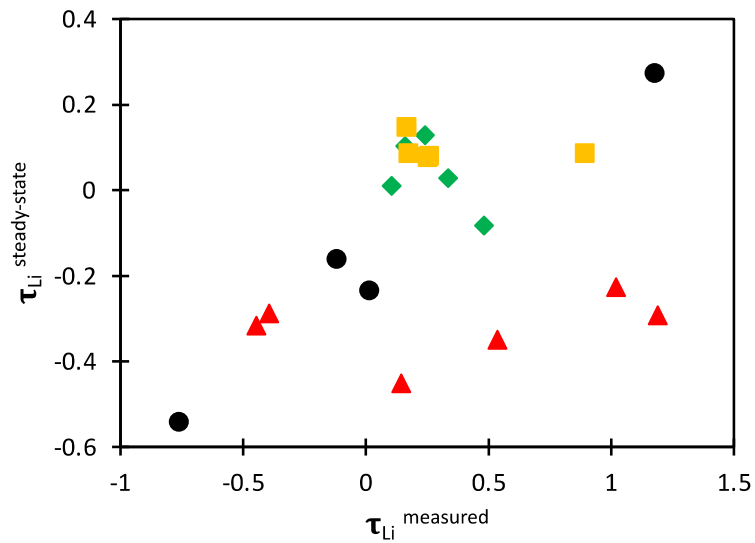
Figure 7. Comparison of measured τ_{Li} values, compared to steady-state τ_{Li} values calculated from Li isotope ratios (Bouchez et al., 2013). Co-variation (as for HA soils) would suggest that depletion or enrichment may be due to weathering intensity, while no correlation (as for the other soils) suggest decoupling between processes controlling soil and present-day water composition. See text for details. Symbols are the same as figure 6.

1017
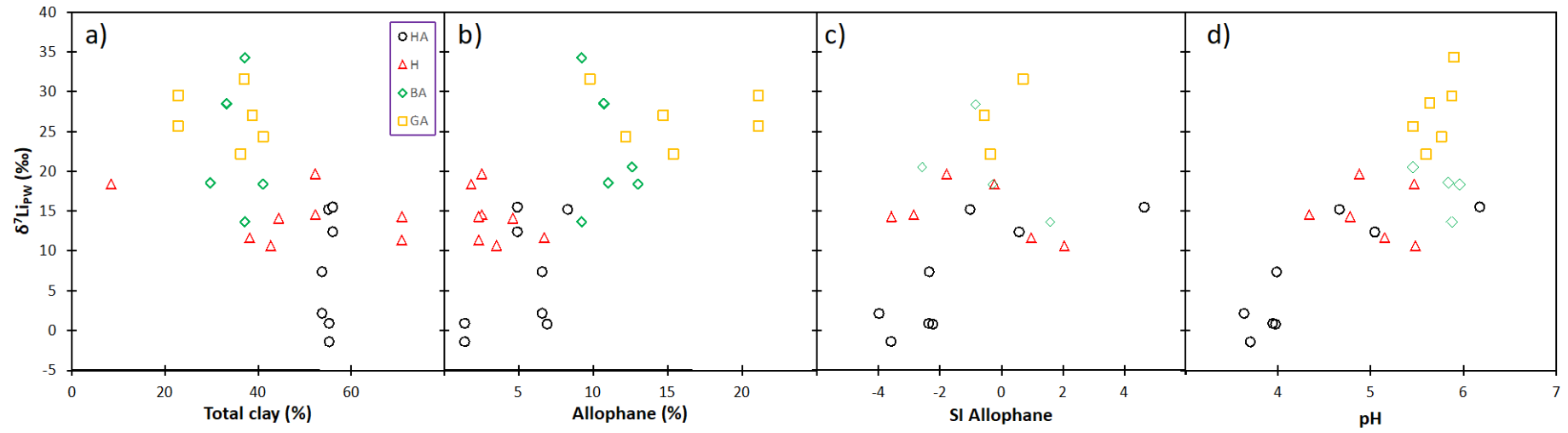
1019   Figure 8. Pore water Li isotope ratios as a function of soil total clay content (a), soil allophane content (b), and the PHREEQC-derived allophane

1020   saturation index (c), and pH (d).
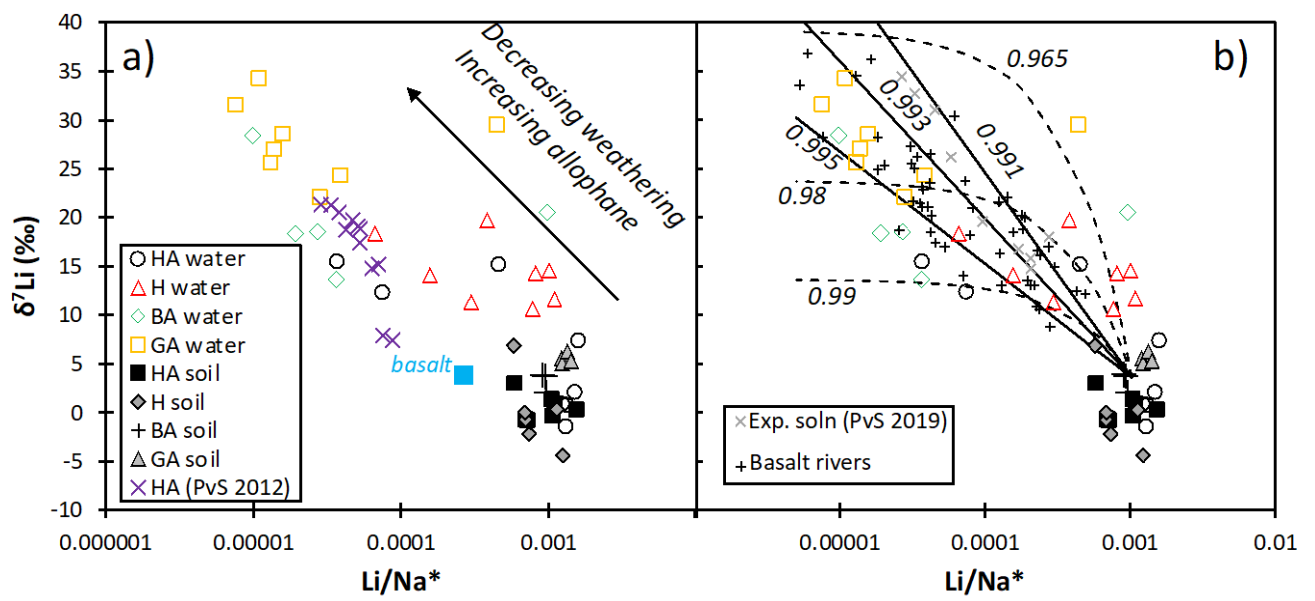
1021

1022

1023

1024

1025

1026

1027
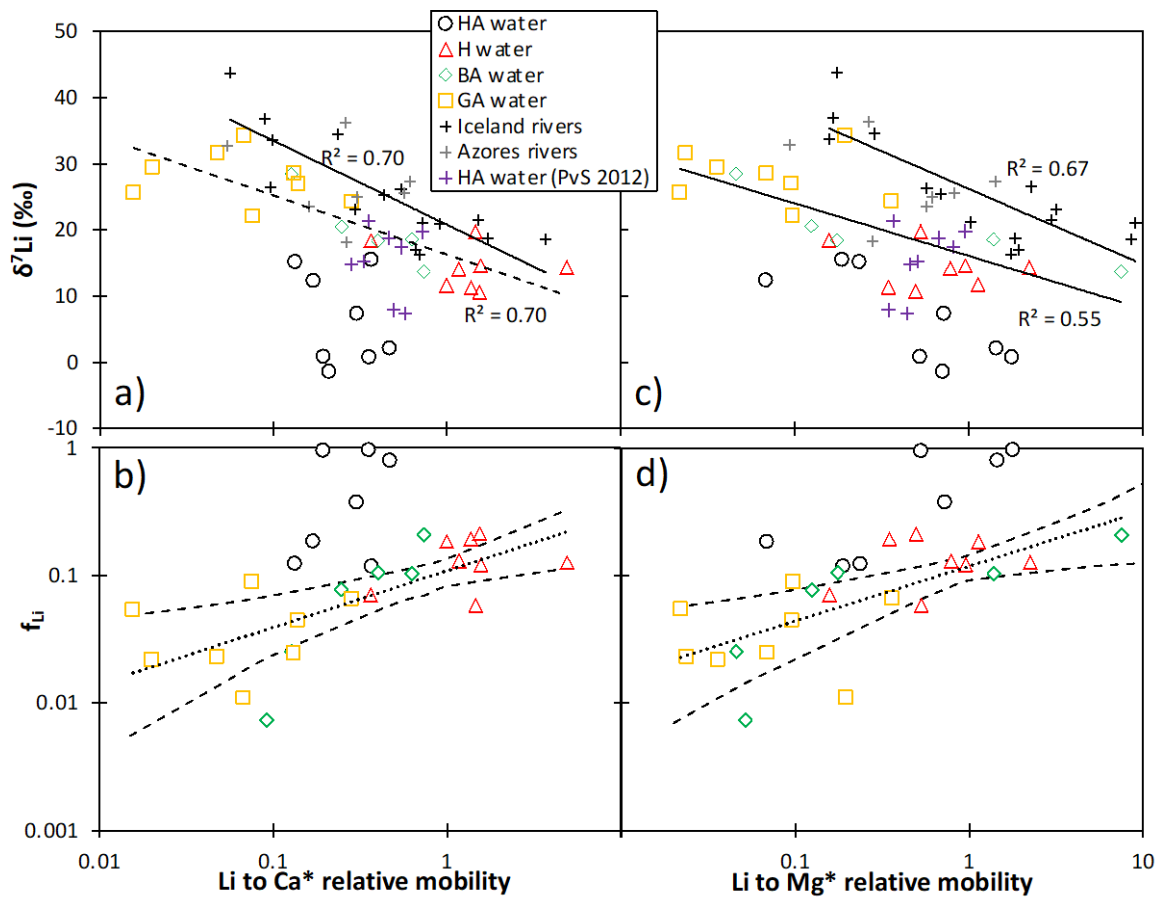
1028

1029

1030

1031

1032

1033

1041
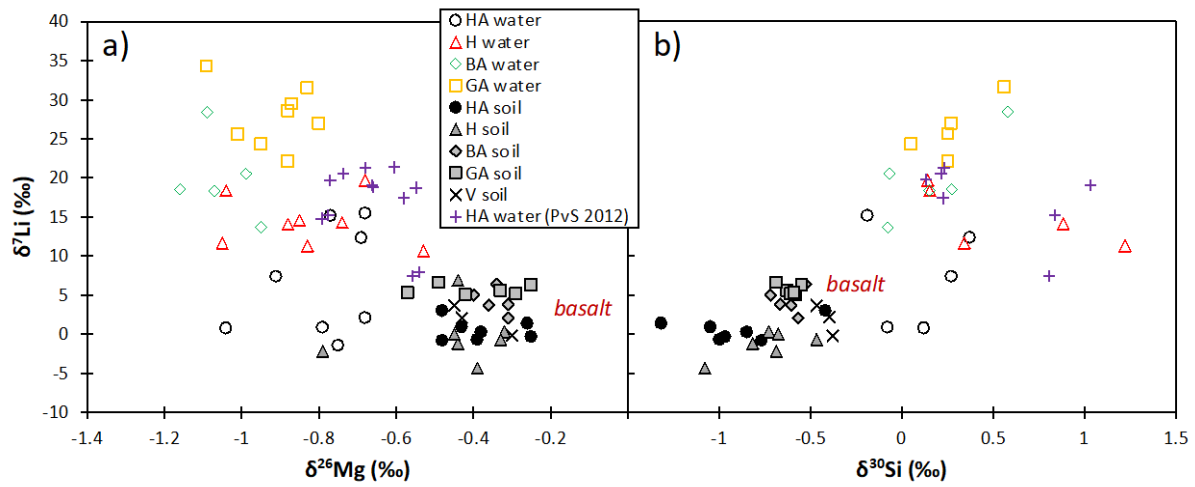
1042

1043

1044

1045

1054

1055

1056

1057

1058   Figure 11. (a) Li isotope ratios as a function of Mg isotope ratios (Opfergelt et al., 2014;

1059   Pogge von Strandmann et al., 2012); (b) Li isotopes as a function of Si isotope ratios

1060   (Opfergelt et al., 2017b; Pogge von Strandmann et al., 2012).

1062

1063

1064

1065

1066

1067

1068

1069

1070

1071

1072

1073